06-6555/1

(1)

FRACTURE MICROMECHANICS OF CONTINUOUS FIBER AND TEXTILE REINFORCED METAL AND CERAMIC MATRIX COMPOSITES

Prepared by

D. L. Davidson

INTERIM TECHNICAL REPORT
N000014-93-C-0040

Prepared for

Office of Naval Research
800 North Quincy St.
Arlington, VA 22217

February 1994

SOUTHWEST RESEARCH INSTITUTE
SAN ANTONIO
DETROIT
HOUSTON
WASHINGTON, DC

REPORT DOCUMENTATION PAGE

Form Approved
OMB No. 0704-0188
Exp.Date: Jun 30, 1986

1a. REPORT SECURITY CLASSIFICATION UNCLASSIFIED	1b. RESTRICTIVE MARKINGS
2a. SECURITY CLASSIFICATION AUTHORITY	3. DISTRIBUTION/AVAILABILITY OF REPORT Unlimited
2b. DECLASSIFICATION/DOWNGRADING SCHEDULE	
4. PERFORMING ORGANIZATION REPORT NUMBER(S)	5. MONITORING ORGANIZATION REPORT NUMBER(S) 4313283-02
6a. NAME OF PERFORMING ORGANIZATION Southwest Research Institute 6b. OFFICE SYMBOL (If applicable)	7a. NAME OF MONITORING ORGANIZATION Dr. Steven G. Fishman - Code 1131 Office of Naval Research
6c. ADDRESS (City, State, and ZIP) 6220 Culebra Road, P.O. Drawer 28510 San Antonio, TX 78228-0510	7b. ADDRESS (City, State, and ZIP Code) 800 North Quincey Street Arlington, VA 22217-5000
8a. NAME OF FUNDING/SPONSORING ORGANIZATION Office of Naval Research 8b. OFFICE SYMBOL (If applicable)	9. PROCUREMENT INSTRUMENT IDENTIFICATION NUMBER N00014-85-C-0206
8c. ADDRESS (City, State, and ZIP) 800 Quincey Street Arlington, VA 22217-5000	10. SOURCE OF FUNDING NUMBERS PROGRAM ELEMENT NO. / PROJECT NO. / TASK NO. / WORK UNIT ACCESSION NO.

11. TITLE (Include Security Classification)

Fracture Micromechanics of Continuous Fiber and Textile Reinforced Metal and Ceramic Matrix Composites

12. PERSONAL AUTHOR(S)

13a. TYPE OF REPORT	13.b TIME COVERED	14. DATE OF REPORT (Year, Month, Day)	15. PAGE COUNT
	FROM 4/93 TO 2/94	94/02/17	52

16. SUPPLEMENTARY NOTATION

17. COSATI CODES			18. SUBJECT TERMS (Continue on reverse if necessary and identify by block number)
FIELD	GROUP	SUB-GROUP	Key Words: Metal matrix composites, ceramic matrix composites, continuous fiber reinforcement, fatigue crack growth, crack growth mechanisms, woven fiber reinforcement

19. ABSTRACT (Continue on reverse if necessary and identify by block number)

This report summarizes progress on fatigue crack growth through unidirectional SCS-6/titanium alloy composites and the fatigue and fracture of ceramic matrix composites reinforced with continuous fibers, both large and small, in unidirectional and woven forms. The fiber/matrix interaction is detailed for SCS-6/titanium alloy composites near stress concentrations, and it is shown how that is similar to measurements of fiber stress in the wake of fatigue cracks. The main theme of the work on ceramic matrix composites is the effect of fiber architecture on fatigue behavior.

20. DISTRIBUTION/AVAILABILITY OF ABSTRACT [ ] UNCLASSIFIED/UNLIMITED [X] SAME AS RPT. [ ] DTIC USERS	21. ABSTRACT SECURITY CLASSIFICATION Unclassified
22a. NAME OF RESONSIBLE INDIVIDUAL	22b. TELEPHONE (Include Area Code) (210) 522-2314 22c. OFFICE SYMBOL

DD FORM 1473 84 MAR

83 APR edition may be used until exhausted.
All other editions are obsolete.

EXECUTIVE SUMMARY

This report summarizes our research accomplishments on the fatigue and fracture of titanium matrix and ceramic matrix composites. The work on the titanium composites is nearly complete, while the research on the ceramic matrix composites continues, with emphasis on woven fiber reinforced materials. Research on the interaction of fibers with matrix near stress concentrations and cracks is summarized in a manuscript submitted for publication at ASTM while the research on the ceramic composites is summarized in a pre-manuscript that will be finished within the next year.

Fibers were found to debond and slip relative to the matrix at stresses well below the fiber fracture stress near hole and slit stress concentrations. This same behavior was found for fibers bridging fatigue cracks. The debonding and slipping of fibers near a stress concentration caused stress to be distributed more equally between other fibers and matrix where slip had not yet occurred. For a fatigue crack, fiber/matrix slip equalized the stress in the bridging zone and allowed prediction of crack growth rate using a relatively simple fracture mechanics approach. The analytical treatment of fiber/matrix behavior near holes and slits is limited, but there was general agreement between existing analyses and the experimental findings.

Experiments have been conducted on ceramic matrix composites having three different fiber architectures. These materials were also manufactured using three different methods: large and small unidirectional fibers and woven small fibers. There is general similarity between the failure mechanisms in fatigue for the large and small fiber unidirectionally reinforced composites, but there are significant differences in detail. Cracks could not be made to grow approximately perpendicular to the stress axis from notches in the Nicalon/CAS composite. This behavior is completely unlike any other material for which I have seen published reports or personally examined. Crack growth rate was not a definable parameter for this composite, but it was for the other materials.

Research into the failure mechanisms for the materials with woven reinforcement will continue. The material tested thus far, which exhibited "plastic-like" behavior even though it was composed of two brittle components, had a relatively high fracture toughness and is generally damage tolerant. The origins of this apparent plasticity will be sought, and fatigue properties will be further investigated.

TABLE OF CONTENTS

LIST OF FIGURES
(Paper)

LIST OF FIGURES
(Report)

1. INTRODUCTION

This report consists of two manuscripts, one complete and in review for publication, and the other still being completed. The first manuscript [1] details the experimental technique used to determine fiber stresses in titanium alloy matrix composites. Results are given for fiber stresses measured near hole, slit, and crack stress concentrations. Finally, it is shown that our previously published [2] direct measurements of fiber stresses in the wakes of fatigue cracks are similar to the results obtained by other investigators using indirect methods. The implications of these measurements for prediction of fatigue crack growth rates are also discussed.

The second part of this report [3] compares the fracture behavior of several ceramic matrix composites having different fibers and fiber architectures. These differences in fiber arrangement and size required different manufacturing methods and each had a different matrix material. This manuscript is still being prepared for publication, but will be sent for review in the next few months.

2. FATIGUE CRACK GROWTH THROUGH CONTINUOUS FIBER METAL MATRIX COMPOSITES

During the past year, work was concluded on these materials for several reasons:

(1) The fracture mechanics framework published in ref. [2] for predicting the rate of crack growth through SCS-6/Ti-6Al-4V at ambient temperature has been confirmed by Larsen and co-workers at Wright-Patterson AFB [4], and other, more tangential, published work has been interpreted as supporting the conclusions of ref. [2].

(2) Previous work on fatigue crack growth through ARALL (aramid fiber reinforced aluminum alloy) [5] was found to support the same concepts as derived for the titanium matrix composites [6].

(3) For the SCS-6/Ti-6Al-4V composites to be fatigue crack tolerant, stresses must be less than 25% of yield, which would impose an operating stress that is unacceptably low for these composites from an economics and design viewpoint; therefore, it is doubtful that they would be used at a stress level where a fracture-mechanics-based damage tolerance methodology is applicable for determining lifetime.

(4) Fatigue crack growth through a Ti-14Al-21Nb (intermetallic) matrix composite exhibited nearly the same behavior as the Ti-6Al-4V matrix composite. Although microstructurally there were differences between these

two materials, they were insufficient to warrant a more detailed examination because the fracture mechanics of fatigue crack growth would be very similar to the study already completed.

(5) At 650°C, the SCS-6/Ti-6Al-4V composite was found to be creep dominated (crack opening displacement (COD) was time dependent). When the temperature was lowered to 600°C, this time dependence of COD ceased, but fatigue crack growth through the composite was much the same as at ambient temperature. It was concluded that the use temperature for this material would be below the creep dominated level; thus, a special study of fatigue crack growth at 600°C would not be of particular interest.

The paper prepared for publication in an ASTM-STP is reproduced in the following pages.

Life Prediction Methodology for Titanium Matrix Composites
Hilton Head Island, SC, March 22-24, 1994

FIBER-MATRIX MICROMECHANICS AND MICROSTRUCTURAL OBSERVATIONS UNDER TENSILE AND CYCLIC LOADING

D.L. Davidson
Southwest Research Institute
San Antonio, Texas

ABSTRACT: A technique is described for measuring the displacements in fibers due to loading the composite. Fiber access was obtained by removing only very small pieces of the matrix, thereby minimizing the change in residual stresses. Fiber stresses were obtained near a hole, a slit and a fatigue crack. It was found that fibers slipped within the matrix at a stress of 2 - 2.6 GPa near both the hole and slit; after cyclic loading the specimen with a hole, fiber stress at slip increased to 2.6-3.6 GPa. Fiber stresses bridging the wake of a fatigue crack were found to be approximately constant. The models used to compute a stress intensity factor at the tip of a bridged fatigue crack are reviewed, and it is shown that those assuming a constant fiber stress gave the best results.

KEY WORDS: fiber stress, stress concentration, fatigue crack growth, *in-situ* measurements, stereoimaging, bridging zone fiber stress distribution

Introduction

A load applied in the fiber direction of continuous fiber metal matrix composite is shared by matrix and fiber. To determine analytically how the load is partitioned between fiber and matrix, it is necessary to assume elasticity and nonslippage between fiber and matrix. Fibers in these composites have a higher modulus than the matrix, and, therefore, will carry an increasingly higher load than the matrix which causes an increasingly larger shear stress at the fiber-matrix interface to occur. Thus, as the load is increased, either the fiber-matrix interface will break and interfacial slip will occur, or the fiber will break.

The methods developed for determining the point at which a fiber will separate from the matrix are: (1) the fiber pushout test [1], and (2) the fiber pullout test [2]. The value of these seemingly simple, direct methods

of measurement is that the results should be easily interpreted, but experience has shown that the tests are more complex than they appear and that considerable analysis may be required to interpret the measurements [3]. One of the disadvantages of both of these testing methods is that the composite must be extensively altered to obtain specimens suitable for making the measurements.

The limitations in the fiber pushout and pullout tests has led to the development of an alternative solution for determining the response of fibers to loading. Ideally, any new method would circumvent the limitations imposed by the pushout and pullout tests, which is the need for extensive material removal to expose the fibers for either pushing or the attachment of a tensile loading fixture. Extensive removal of material for testing purposes alters the residual stress state of the material, which is important because it is the compressive radial residual stress that provides a force normal to the fiber-matrix interface that regulates the debonding and slippage of the fiber. This paper describes briefly a technique developed for the *in situ* observation of fibers that removes only a small amount of matrix, and, therefore, results in very little alteration of the residual stress state.

Specimens prepared for the observation of fibers *in situ* were remotely loaded through pins on the centerline of the specimen. The response of fibers to loading was determined by comparing photographs made minimum load with those made at increasing load using the stereoimaging technique [4]. This allowed the visual system (eye and brain) to see the displacements in fiber and matrix caused by the application of load. Those displacements were measured using our system for automated photogrammetry, termed DISMAP [5]. The response of fibers to loading was observed *in situ* in specimens having a variety of stress concentrations, i.e., holes, notches, slits, and fatigue cracks, and the results from those experiments are given following a description of the technique used to access the fibers.

Description of Technique

To reveal fibers for observation, the matrix overlaying the first row of fibers was removed, very carefully, exposing as small a portion of the fiber as possible, and thereby perturbing the residual stresses in the composite to the minimum extent. The resulting hole in the matrix that exposes the fiber has been termed a "fiber port." Matrix removal was accomplished

most successfully using a combination of ion etching and electropolishing, but some fiber ports were made using only electropolishing. The fiber port preparation sequence used is depicted in Fig. 1.

Ion etching was used to provide a trench with well defined sides perpendicular to the fiber direction, Fig. 1(a). The mask used to limit the region etched by ions was two parallel razor blades separated by 0.5 mm. Nitrogen ions at approximately 8 KeV were used to make a trench varying in depth from about 0.1 mm to almost 0, with the deepest part of the trench near the stress concentration. Each trench required several days of ion etching time. The resulting trench width was somewhat less than the 0.5 mm separation of the masks.

After ion etching, the specimen was masked off completely with stopoff lacquer, except for the trench emanating from the stress concentration. The sharp discontinuity of the ion etched trench allowed the high viscosity lacquer to be stopped exactly at the edge of the trench, resulting in only a narrow region of matrix left exposed to the polishing solution.

Electropolishing was accomplished on all the titanium alloy matrix materials using nitric acid in ethanol, usually with a concentration of 25 vol. %. The best polishing results were obtained with a potential of between 20 and 22 vdc. in a solution maintained at a temperature of -20 to -40°C. Matrix material was very carefully dissolved by using small time increments for electopolishing that varied from 30 sec. to 2.5 min. Between each increment, the specimen was examined under a microscope for evidence of fibers.

The specimen was first electropolished with the trench in the vertical position with the stress concentration at the top. This position caused the thickness of the viscous layer to increase with distance from the stress concentration because gravity caused the heavier viscous layer to flow downward. Thus, the highest polishing rate occurred at the top of the trench, nearest the stress concentration where the viscous layer was the thinnest.

As soon as enough matrix was removed to reveal the first fiber, this portion of the specimen was masked with lacquer. Then, the specimen was turned 90° so that the trench was perpendicular to the force of gravity. This meant that the viscous layer was thicker in the lower part of the

trench and drained uniformly along its length. Thus, polishing occurred fastest in the upper part of the trench. This manipulation of specimen position allowed the size of the fiber port to be controlled better than if one position alone had been used. Ports made using the method described ranged from 35 to 350 μm in length, with the typical port being elliptical with axes of 150 μm by 60 μm.

The surfaces of the fibers revealed through the fiber ports were relatively smooth and featureless, as viewed by secondary electrons in the scanning electron microscope (SEM), and that would have caused difficulty during the observation and measurement of fiber response to loading. This problem was solved in two ways: A light ion etch was used to texture the fiber surfaces, or magnesium oxide particles were deposited from smoke on the fiber surfaces. Both of these treatments gave the fiber surface a fine texture when viewed using the secondary electron image in the SEM. Some of the fiber ports made using this process are shown in **Fig. 2**. Fibers in the case illustrated were decorated with MgO particles.

Loading of specimens in which fibers were exposed through fiber ports was accomplished using a special stage that fit within the specimen chamber of a SEM [6]. With this equipment, load was applied to both ends of the specimen using hydraulic actuators and the fibers were observed under high resolution conditions. An illustration of the displacements measured in and near a fiber is shown in **Fig. 3**.

Results

Observations of fiber response were made under both unidirectional monotonic loading and after cyclic loading. All specimens used were straight sided, 25.4 mm wide by 54 mm long and 0.94 mm thick. The stress concentrations were located symmetrically about the centerlines of the specimen. Loading was through 6.3 mm holes located along the specimen long axis centerline about 30 mm apart. The specimens loaded monotonically had a Ti-15V-3Al-3Cr-3Sn (wt.%) matrix reinforced with 35.5 vol.% Textron Corp. SCS-6 fibers (≈ 150 μm diameter). The fatigue cracked specimens were Ti-6Al-4V matrix reinforced with 42 vol.% SCS-6 fibers. Both composites were manufactured by Textron Specialty Materials using the foil-fiber-foil method. Fiber architecture was different for the two composites used, although for both there were 4 fiber layers. The Ti-15-3-3-3 matrix specimens had two inner fiber layers transverse to the loading axis. Thus, only the 2 outer layers were parallel to the direction of

loading. The Ti-64 matrix specimens had all 4 fiber layers oriented in the direction of loading.

Stress concentrations examined in the SCS-6/Ti-15-3 specimens were: (1) a HOLE 12.5 mm in diameter and (2) a SLIT 14.1 mm in length (1.61 mm longer on the side of the specimen having fiber ports) and 0.28 mm wide. Specimens of SCS-6/Ti-64 were FATIGUE cracked from centered slits approximately 8 mm long by about 0.5 mm wide. A complete description of the fatigue specimens can be found in ref. [7].

The technique used to determine fiber stress was as follows: Photographs of the fibers were made at minimum load through the fiber port holes, and then again with increasing load. Displacements were measured with DISMAP and converted into strains, which were then multiplied by the modulus of the fiber (400 GPa) to obtain stress.

HOLE Specimen Monotonically Loaded During loading of hole specimen, the first fiber broke at a low load; it was probably damaged during specimen fabrication. The responses of the second fiber (0.39 mm from the hole edge) and third fiber (0.60 mm) were followed in detail. The fiber stresses shown in **Figs. 4 (a and b)** are given as a function of the applied load. The figures show that the fiber (strain) stress increased with load to approximately (0.0056) 2.5 GPa, but either remained constant or decreased as load was further increased, then fiber (strain) stress again increased as the applied load increased.

An abrupt change in slope of fiber stress vs. load is interpreted as an indication that sufficient slip has occurred between the fiber and matrix to transfer part of the fiber stress to the matrix and other fibers. Slip may have initiated at a lower load, but it was insufficient to transfer enough load from the fiber to drastically alter its load-strain relation. Thus, for loads sufficient to cause a fiber (strain) stress of about (0.0056) 2.5 GPa, considerable debonding between fiber and matrix is likely to have occurred.

SLIT Specimen Monotonically Loaded Stresses in the 3 fibers nearest the slit (0.17, 0.37, and 0.55 mm from the slit, respectively) were measured. The stress vs. load history for these fibers, **Figs. 5 (a,b and c)**, is similar to that found for fibers near the hole specimen, except that there is more of what might be interpreted as stick-slip behavior. Stress (strain) at the point of first slippage with increased loading varied between 2 GPa (0.0049) and 2.65 GPa (0.0066), which is about the same level as found for

the hole specimen.

Irregularities in fiber slippage with increased loading could occur for at least two reasons: (1) surface irregularities on the interfaces between fiber coating and matrix or between the fiber and its coating could cause the fiber to slide easier at some points than at others, (2) sliding may be occurring at both interfaces (fiber/coating or coating/matrix), and (3) the load transfer between the various slipping fibers and their surrounding matrix is likely to be a complex interactive process.

HOLE Specimen Cycled 30 times A second HOLE specimen was cycled 30 times between 150 and 4250 N. Cycling did not break any of the fibers that were being observed, although the loads should have been large enough to strain the fibers well beyond the point where slippage occurred between fibers and matrix. A number of load cycles were applied to bring to equilibrium some of the complex load redistribution between fibers and matrix and possibly smooth some of the interfacal roughness that might affect the load transfer. Strains in the first 3 fibers (0.13, 0.27, and 0.47 mm from the hole edge, respectively) were measured, as shown in **Figs. 6 (a, b and c)**. The same complex behavior found for fibers in the monotonically loaded hole is still evident for fibers 2 and 3, but for fiber 1 there may have been some change. For all the fibers, the stress at first unloading was 3.2 - 3.6 GPa, which is greater than the ~ 2.2 GPa found for the monotonically loaded hole specimen. For both hole specimens, the number of stick-slip events observed was less than for the slit specimen.

Summary of Hole and Slit Specimen Results The fiber stress levels at which slippage occurred between fiber and matrix are summarized in **Table 1** and compared to the average stress that a fiber would have supported for the load applied when slippage began. The average stress was calculated on the basis of net section area, i.e., ignoring the area of the stress concentration. The stress concentration factor tabulated in the last column was determined by dividing measured fiber stress by the average stress.

The stress concentration for the hole is very large compared to that expected at a hole in an isotropic material (about 4.3, as determined from Peterson [8]); however, the analysis by Bigelow [9] indicates that fiber stresses should be in the range 1.1 to 1.8 GPa for the applied stresses used in these experiments, which would give a first fiber stress concentration of 7 to 14, somewhat below the 14-17 found experimentally.

For the specimen with a slit, the stress concentration found (13 to 18) is about that expected based on elastic analysis, Peterson [8], for an elliptical notch in a homogeneous solid with a height-to-width ratio of 8 ($K_{tg} \approx 20$). Also, the results of a three-dimensional finite element analysis by Johnson and Bigelow [10] for a slit of similar dimensions indicated that a stress concentration of 22 in the first fiber would be expected. Thus, the experimental results for the slit are about what should was expected.

Table 1--Hole and Slit Results Summary

Stress concentration	Fiber	Load	Slip stress	Avg. stress	Stress concentration factor
		-N-	----GPa----		
Hole 2	2	2500	2.2	0.162	14
	3	2000	2.2	0.130	17
Hole 1	1	2000	2.6	0.130	20
(cycled 30 times	2	2200	3.5	0.145	25
at 170 MPa)	3	2200	3.6	0.142	25
Slit 2	1	2000	2.6	0.130	18
	2	2000	2.0	0.130	13
	3	1800	2.2	0.116	17

The increase in stress concentration caused by cycling the hole specimen evidently occurred due to the rearrangement of applied load between the fiber and matrix. Residual stresses in the matrix (tensile) and fibers(compressive) were relaxed due to cycling the hole specimen, and this resulted in the fibers carrying an increased load, thereby increasing the stress concentration. Fiber stresses may be smaller than measured for the uncycled hole and slit specimens because at minimum load the fibers were in compression. Conversely, if cycling redistributed the stresses as expected, the fiber stresses at minimum load would be close to zero. Thus, the fiber stress concentrations for the cycled hole specimen could be more than given in the table. An analysis [9] of the first fiber stress concentration after 200,000 tension load cycles at a stress of 250 MPa indicated that the stress had increased by a factor of 2 (from 1.1 to 2.2 GPa) for an applied stress of 140 MPa. Experimentally, fiber stress increased by a factor of 1.4, which is lower than that predicted, but transfer of load from matrix to fiber was as predicted by the analysis.

FATIGUE Specimens Only 2 of the 4 specimens in which fatigue cracks were grown was prepared with fiber ports. Extensive fiber bridging was observed for these specimens at some levels of applied stress. Fiber strains were measured both ahead of and behind the crack tip. Fiber strains were measured only at maximum load as a function of crack length, applied stress level, and the extent of fiber bridging. Table V of ref. [7] lists all the measured fiber strains (converted to stress through multiplying by the modulus). These data are shown in **Fig. 7** as a function of position relative to the crack tip. The scatter in these data are indicative of: (1) errors in the measurement of fiber strains (shown by the error bars), (2) of the irregularities in stress caused by differences in fiber/matrix interface, (3) of irregularities in fiber spacing within the matrix, and probably some other factors.

Fatigue cracks were grown at applied stresses between 118 and 175 MPa, and bridging lengths varied from 1 to 2.4 mm. Fibers stresses, taken separately for each combination of variables, or collectively as shown in the figure, do not show any effect of applied stress or location relative to the crack tip. Applied stress had such little effect on fiber stress because of differences in bridging length. The important result shown in the figure is the insensitivity of fiber stress to distance from the crack tip.

A simple method was devised to compute the expected fiber stresses, based on applied stress, crack length, and length of the bridging zone. The remotely applied load was assumed to partition in proportion to the cracked and uncracked cross sectional areas, and fiber stress was assumed to be uniform in the bridging zone and support the entire load of the cracked area [7]. The fiber stresses thus computed (see Table V of [7]), agreed with those measured reasonably well, as shown in **Fig. 8**.

Discussion

The levels of fiber stress and their distribution relative to the fatigue crack tip are not surprising when the stresses in fibers near the other stress concentration geometries are considered. For both the hole and slit specimens, load application caused a redistribution of fiber stresses because of slippage between fiber and matrix. Whereas the amount of slippage was not determined for the hole and slit specimens, it was measured for the fatigue cracks [7]. Repeated cycling of the slipping interface damaged the fiber coating, so that when the surrounding matrix

was removed chemically, spallation and cracking in the coating were evident. The damage zone was easily measured, and it was found that the extent of slip was a function of the crack opening displacement, which increased with distance from the crack tip. This finding indicated that fiber stresses that would have been high because of their distance from the crack tip were lowered by an increase in slip distance between the fiber and matrix. Therefore, fibers bridging the crack tended towards constant stress in the equilibrium condition brought on by the application of many thousands of cycles. This result has been reinforced by a number of other investigators, as will be reviewed later.

Fiber coating damage that increased with distance from the crack tip has been reported also by Blatt, et al. [11], using a nondestructive technique.

The results of the fiber stress measurements also indicate the mechanism of fiber fracture. The extensive damage to the interface caused by growing the fatigue crack lowered the load transfer characteristics of the interface in the damaged region to a level that significant load transfer within the slip zone is unlikely. Rather, load transfer to the fibers was occurring mainly beyond that point in the region of elastic interaction between fibers and matrix. Thus, the fibers were approximately free of load transfer within the slip zone, so that as distance to the crack tip increased with a longer bridging zone, the length of fiber subjected to a high stress increased. Since fiber strength is inversely proportional to the length being stressed, fiber fracture became more likely as distance from the crack tip increased. Thus, the length of the bridging zone would be expected to be limited under steady state crack growth conditions.

As noted above, in addition to the direct experimental measurements presented by Davidson [7], there is also indirect evidence that fiber stress is constant, or nearly so, in the bridging region behind fatigue cracks. Ghosn, et al. [12], successfully modeled the growth of fatigue cracks in single edge notched (SEN) specimens of SCS-6/Ti-15-3 using a "fiber pressure" approach, which essentially assumed that the fibers within the bridging zone all carried the same stress, but there was a bending component added for the SEN specimen. Later work by these investigators [13] also included a center cracked specimen loaded in tension for which there was no additional bending term. Fiber pressure was calculated as a function of applied stress, crack length, and bridging zone length. Conversely, when the shear lag model [14] was used, the value of interfacial

shear strength (τ) required for agreement between model and experiment was ≈ 6.2 MPa, which is considerably below anything measured.

Bakuckas and Johnson [15] also attempted to use the shear lag theory to rationalize fatigue crack growth data using center notched, unidirectional SCS-6/Ti-15-3 composites. They found that in order to obtain data collapse, the value of τ had to be varied by about a factor of 4, depending on the applied stress, crack length, and bridging zone length.

In another attempt to use the shear lag model to rationalize Davidson's fatigue crack data, Chan [16] assumed that the value of τ decreased as the distance from the crack tip increased due to interfacial damage. Consequently, the values of τ used in his model decreased by a factor of 5 as distance within the bridging region increased to ≈ 1 mm. Kantzos, et al., [17] found that for SCS-6/Ti-15-3, measured values of τ decreased from ≈ 83 MPa to ≈ 55 MPa after 3 loadings using a repeated load pushout test, which is evidence of interfacial damage and wear due to repeated sliding.

Fatigue crack growth rates through SCS-6/Ti-24Al-11Nb specimens with a central hole were measured by Jira and Larsen [18] and modeled by John, et al. [19] They concluded that the results were best modeled using a fiber stress that was constant in the bridging zone, and that was dependent on applied stress and crack length. Measurement of crack opening displacements (COD) were made as a function of distance from the crack tip using a laser interferometric displacement gage. Those measurements best fit a COD profile computed by assuming that the fiber stress in the bridging zone was a constant ratio of the applied stress. Conversely, the value of τ that had to be assumed for the shear lag model to rationalize crack growth data was dependent on the level of applied stress, in general agreement with the results of Bakuckas and Johnson.

In contrast to the results given above is the work of Walls, et al., [20] who grew fatigue cracks through unidirectional SCS-6/Ti-15-3 center notched specimens and explained their results using the shear lag model, with $15 < \tau < 35$ MPa. However, they also noted that the stress required for interfacial sliding degraded with cycling.

The concept of a constant fiber stress within the bridging zone was extended from titanium matrix composites to ARALL, an aluminum alloy matrix composite reinforced with aramid fibers, by Davidson who used his model [7] to compute the crack tip stress intensity factor (ΔK) for the

composite from applied stress, crack length, and bridging distance. The model collapsed data from the composite to the fatigue crack growth rate line for matrix material [21], and the results were found to be relatively insensitive to bridging length.

The collective results of all of the work referenced above leads to the conclusion that cyclic sliding between fiber and matrix degrades the strength of the interface. To get reasonable results using the shear lag model, this degradation must be included by allowing τ to vary with applied stress, crack length, and distance from the crack tip. However, predictive models for this degradation have not been developed. Also, the magnitudes of τ that must be used are lower than anticipated from pushout test results. Conversely, if a simple model is used to compute a constant value of fiber stress in the bridging region from applied stress, crack length, and bridging length, then the models give crack tip stress intensity factors that collapse composite data onto the growth rate curves for the unreinforced alloy.

Finally, fiber stresses at the point of significant sliding (≈ 2.2 GPa, Table 1) were used in the model of Dollar and Steif [22]. Their model for a fiber being pulled from a half space predicts that slip will begin when stress on the fiber reaches 1.22 σ_0 (σ_0 = the compressive residual stress normal to the fiber caused by differential thermal expansion). Using the measured value of 2.2 GPa would predict σ_0 ≈ 1800 MPa, which does not compare well with the value of ≈ 300 MPa found in Cox, et al. [23]. Conversely, using σ_0 ≈ 300 MPa, the fiber stress at slippage is predicted to be ≈ 0.16 of that measured. It is concluded that this model is inapplicable to the present results.

Summary and Conclusions

A technique has been developed that allows displacements to be measured in fibers within metal matrix composites that are being remotely loaded. Small amounts of matrix are removed, exposing a small part of the fiber surface. Displacements are measured using stereoimaging, from which strain is calculated, then stress, using fiber modulus.

1. The fiber stress concentration near a central hole stress concentration was found to be 14-17, which is somewhat higher than predicted by analysis (8-14). Fibers began to slip relative to the matrix at 2-2.6 GPa. Further loading caused fiber stress to decrease, then increase in a manner characteristic of stick-slip behavior.

2. After the specimen with a hole was cycled 30 times, fibers near the hole were found to sustain 2.6 to 3.6 GPa before slipping, an increase in stress concentration of 1.4 over the uncycled hole, whereas, analysis of a similarly cycled hole specimen predicted an increase of 2 in stress concentration, but to a maximum stress of only 2.2 GPa.

3. The stress concentrations in fibers near the end of a slit were found to be 13-17, which compares well to values of 17-22 determined by analysis.

4. Fiber stresses measured in the bridging zone behind fatigue cracks did not exhibit any trend in magnitude with distance from the crack tip, although the scatter in the measurements was large. It was concluded that fiber stress within the bridging zone was constant. This result was consistent with the effect of load on fiber stress measured near the hole and slit stress concentrations.

5. Fatigue crack growth results were found by a number of investigators to be best modeled using a constant stress in the bridging zone.

6. The concepts developed for predicting fatigue crack growth rate through titanium alloy composites were shown also to predict accurately fatigue crack growth rates in the aluminum alloy/aramid composite ARALL.

7. The shear lag model was found to be inappropriate for describing the growth of fatigue cracks through these composites, because the interfacial shear strength must be varied with applied stress and crack length to obtain a fit of model to experimental results.

Acknowledgements

Support for research on fatigue crack growth came from the Office of Naval Research, Contract No. N000-14-93-C-0040, Dr. S.G. Fishman technical monitor, and support for determining fiber stresses near stress concentrations came from NASA Langley Research Center, Contract L-03581D, Dr. W.S. Johnson technical monitor. John Campbell provided experimental assistance, and Jim Spencer provided the DISMAP measurements. This support and assistance is greatly appreciated.

References

1. Marshall, D.B., and Oliver, W.C. "Measurement of interfacial mechanical properties in fiber reinforced ceramic composites" J. Am. Ceram. Soc., v. 70, 1987, pp. 542-548.
2. Hsueh, C-H. "Interfacial debonding and fiber pull-out stresses of fiber reinforced composites" Mat. Sci. and Eng., v. A123, 1990, pp. 1-11.
3. Hsueh, C-H. "Interfacial friction analysis for fiber reinforced composites during fiber push down (indentation), J. Mat. Sci., v. 25, 1990, pp. 818-828.
4. Davidson, D.L. in Scanning Electron Microscopy/1979/II, SEM O'Hare, IL, 1979. pp. 79-86.
5. Franke, E.A., Wenzel, D.J., and Davidson, D.L. "Measurement of microdisplacements by machine vision photogrammetry (DISMAP)" Rev. Sci. Instruments, v. 62, 1991, pp. 1270-1279.
6. Davidson, D.L. and Nagy, A. "A low frequency cyclic loading stage for the SEM" J. Phys. E, v. 11, 1978, pp. 207-10.
7. Davidson, D.L. "The Micromechanics of fatigue crack growth in Ti-6Al-4V reinforced with SCS-6 fibers" Met Trans. A, v. 23A, 1992, pp. 865-879.
8. Peterson, R.E. "Stress Concentration Factors" Wiley, New York, 1974, pgs. 150 and 196.
9. Bigalow, C.A. "A micromechanics based strength prediction methodology for notched metal matrix composites" Composites, v. 24, 1993, pp. 113-121.
10. Johnson, W.S., and Bigelow, C.A. "Elastic plastic stress concentrations around crack like notches in continuous fiber reinforced metal matrix composites" NASA Tech. Memo. 89093, Feb. 1987, Fig. 15.
11. Blatt, D., Karpur, P., Stubbs, D.A., and Matikas, T.E. "Observation of interfacial damage in the fiber bridged zone of a titanium matrix composite" Scripta Met. and Mat., v. 29, 1993, pp. 851-856.
12. Ghosn, L.J., Kantzos, P., and Telesman, J. "Modeling of crack bridging using a unidirectional metal matrix composite" Int. J. Fracture, v. 54, 1992, pp. 345-357.
13. Ghosn, L.J., Telesman, J., and Kantzos, P. "Specimen geometry effects on fiber bridging in composites" in Fatigue '93, vol. II, J.-P. Bailon and I.J. Dickson, eds., EMAS, Cradley Heath, UK, 1993, pp. 1231-1238.
14. Marshall, D.B., Cox, B.N., and Evans, A.G. "The mechanics of matrix cracking in brittle matrix composites" Acta metall., v. 33, 1985, pp. 2013-2021.
15. Bakuckas, J.G., and Johnson, W.S., "Application of fiber bridging models to fatigue crack growth in unidirectional titanium matrix composites" J. Comp. Tech. and Research (ASTM) (in press).

16. Chan, K.S. "Effects of interface degradation on fiber bridging of composite fatigue cracks" Acta metall. mater., v. 41, 1993, pp. 761-768.
17. Kantzos, P., Eldridge, J., Koss, D.A., and Ghosn, L.J. "The effect of fatigue loading on the interfacial shear properties of SCS-6/Ti based MMCs" in Mat. Res. Soc. Proceedings, vol. 273, 1992, pp. 135-142.
18. Jira, J., and Larsen, J.M. "Crack bridging behavior in unidirectional SCS-6/Ti-24Al-11Nb composite" in Fatigue '93, vol. II, J.-P. Bailon and I.J. Dickson, eds., EMAS, Cradley Heath, UK, 1993, pp. 1085-1090.
19. John, R., Jira, J.R., Larsen, J.M., and Ashbaugh, N.E. "Analysis of bridged fatigue cracks in unidirectional SCS-6/Ti-24Al-11 Nb" in Fatigue '93, vol. II, J.-P. Bailon and I.J. Dickson, eds., EMAS, Cradley Heath, UK, 1993, pp. 1091-1096.
20. Walls, D.P, Bao, G., and Zok, F.W. "Mode I fatigue cracking in a fiber reinforced metal matrix composite" Acta mettall. mater., v. 41, 1993, pp. 2061-2071.
21. Davidson, D.L. "Fatigue crack growth through composites with continuous fiber reinforcement" in Proceedings of ICCM-9, vol. I, A. Miravete, ed., Univ. of Zaragoza and Woodhead Publ. Ltd., Spain, 1993, pp. 571-577.
22. Dollar, A., and Steif, P.S. "Load transfer in composites with a coulomb friction interface" Int. J. Solids Struct., v. 24, 1988, pp. 789-803.
23. Cox, B.N., Dadkhah, M.S., James, M.R., Marshall, D.B., Morris, W.L., and Shaw, M. "On determining temperature dependent interfacial shear properties and bulk residual stresses in fibrous composites" Acta metall. mater., v. 38, 1990, pp. 2425-2433.

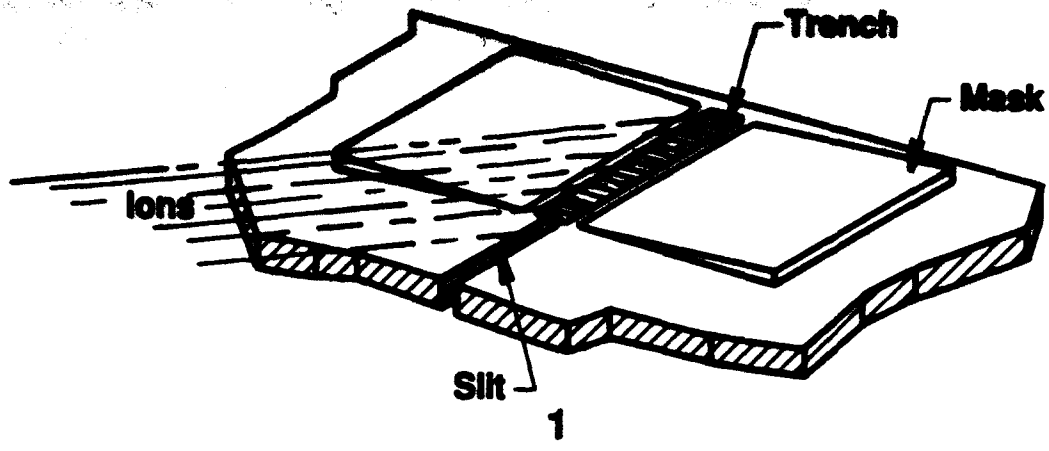

1

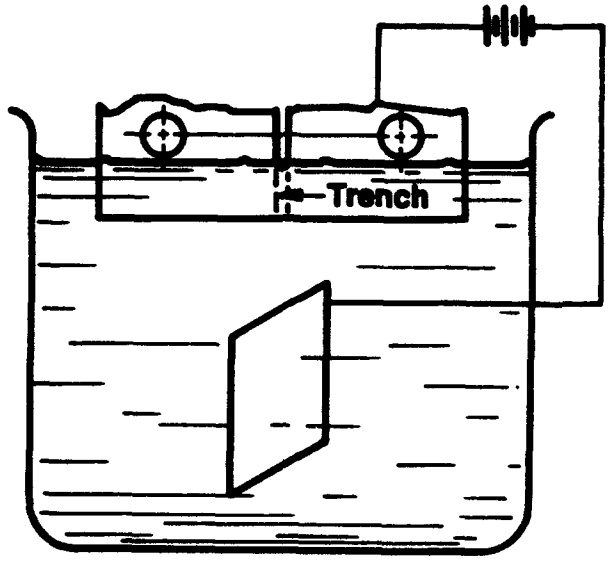

2

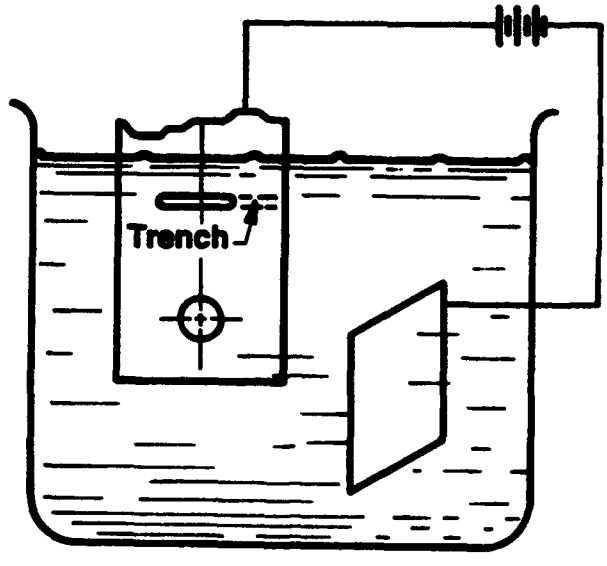

3

Fig. 1 Depiction of the specimen preparation procedure used in creating fiber ports.

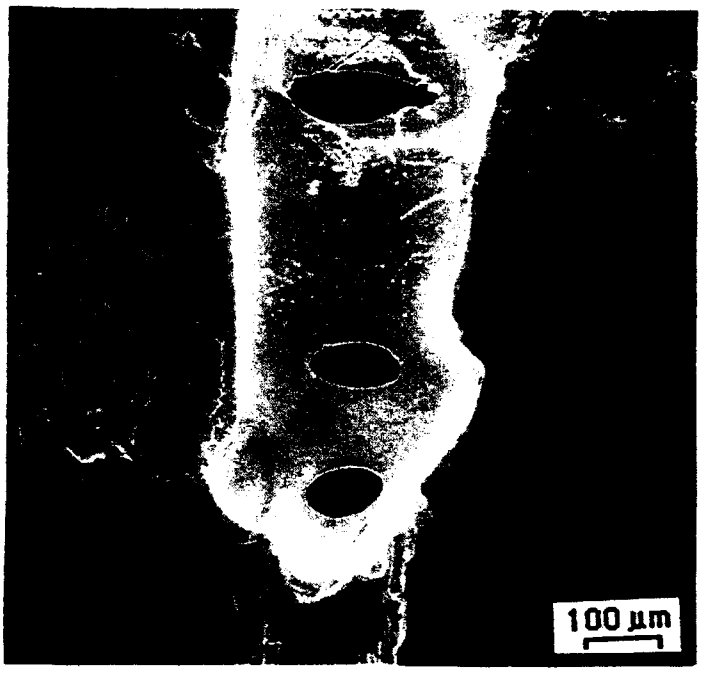

Fig. 2 Illustration of fiber ports prepared using the procedure described in Fig. 1.

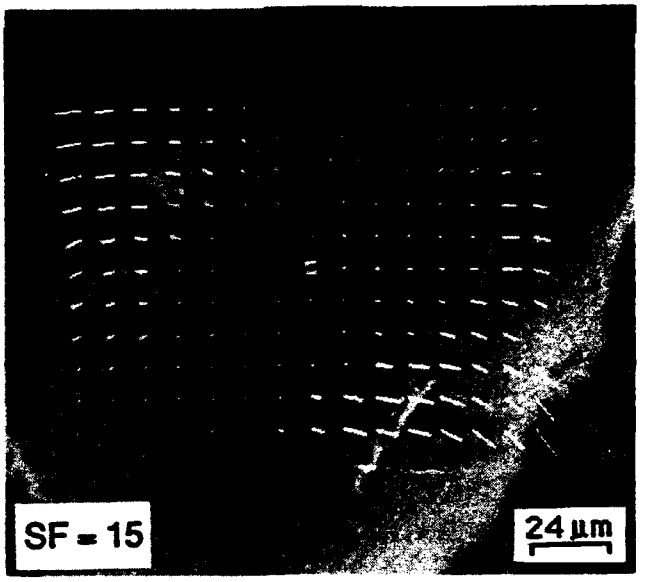

Fig. 3 Displacements in a fiber and the surrounding matrix superimposed on a photograph of the fiber as seen through a fiber port. Displacements were measured each 11 µm, and the displacements are magnified by a factor of 15 for visualization.

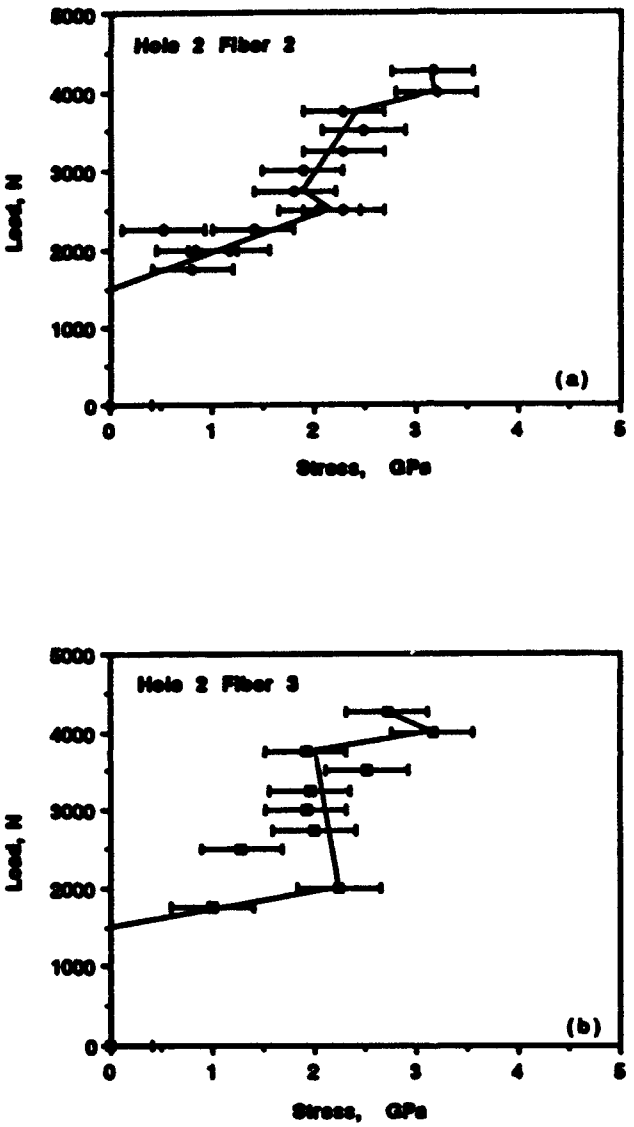

Figs. 4 - (a) Specimen with HOLE: Stress in (a) fiber 2 and (b) fiber 3, as a function of applied load.

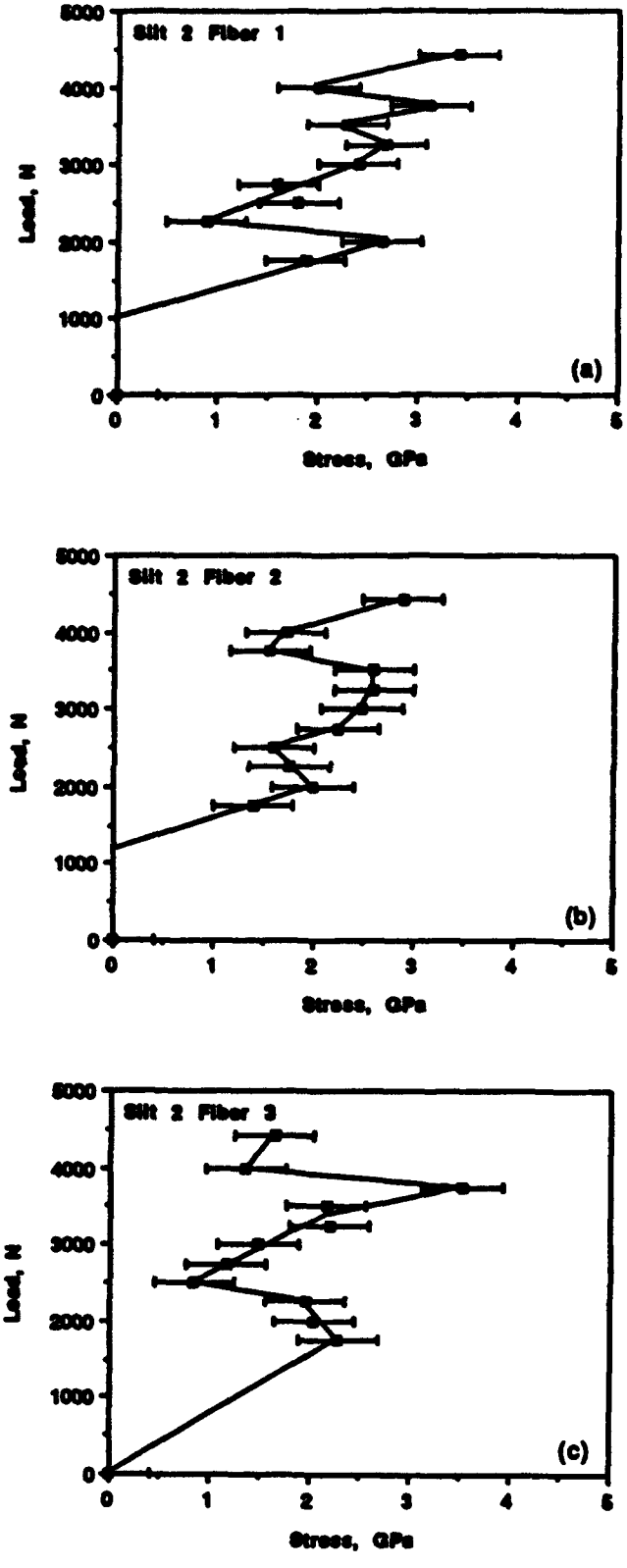

Fig. 5 Specimen with SLIT: Stress in (a) fiber 1, (b) fiber 2, and (c) fiber 3.

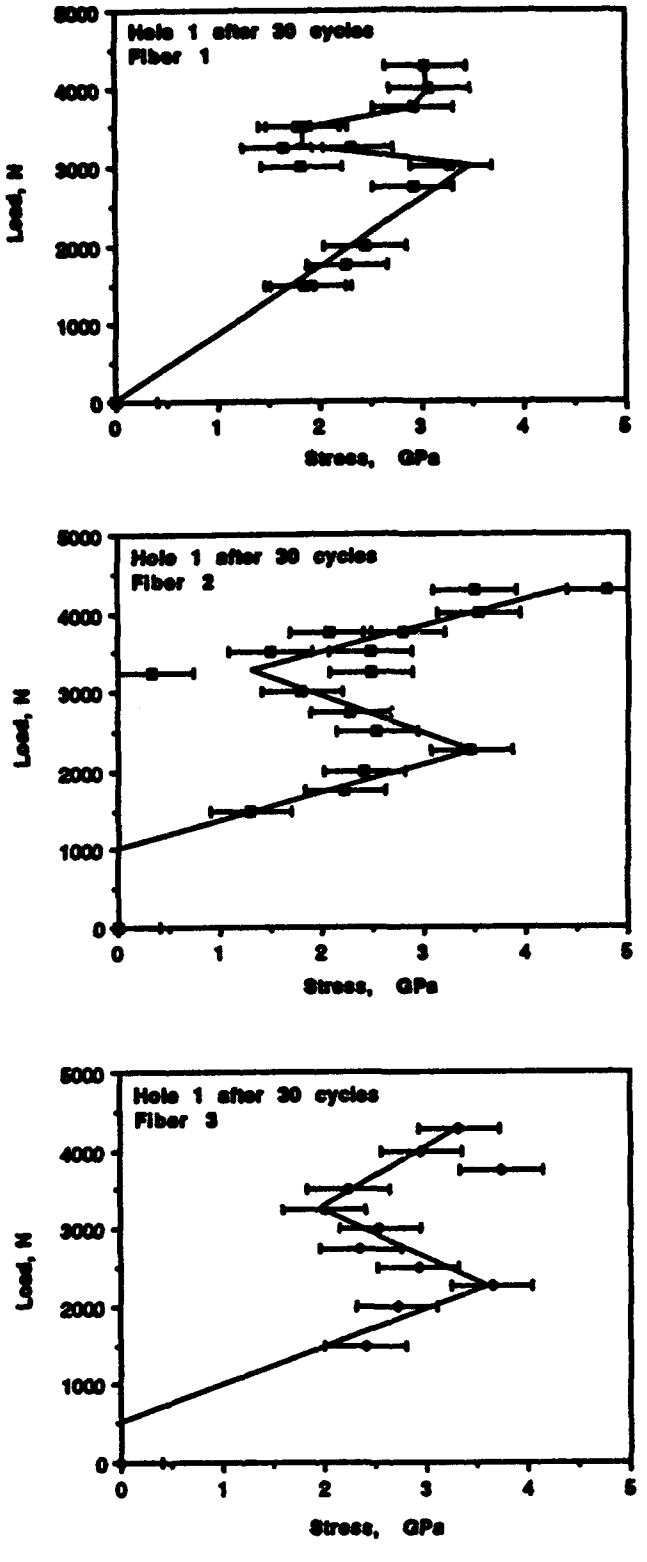

Fig. 6 Specimen with HOLE cycled 30 times at a stress of 170 MPa: (a) fiber 1, (b) fiber 2, and (c) fiber 3.

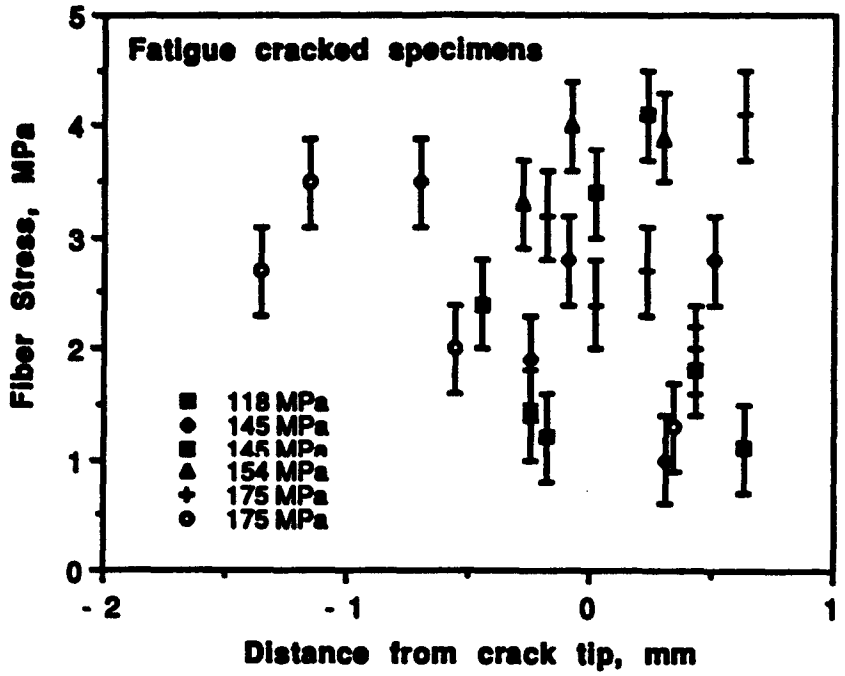

Fig. 7 - Fatigue cracked specimens: Fiber stress as a function of distance from the crack tip. Symbols denote the gross section applied stress on the specimen. See [7] for further details.

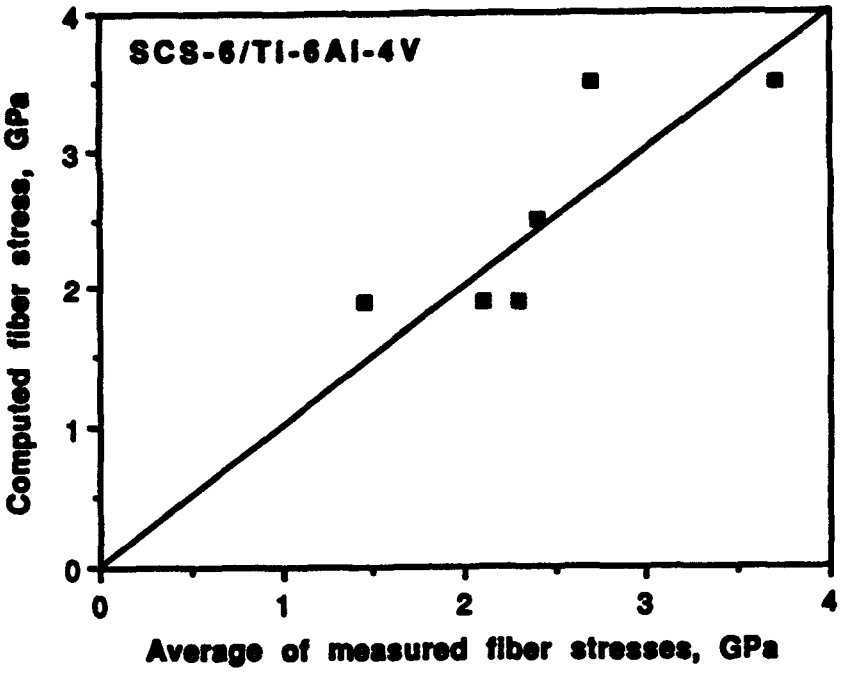

Fig. 8 Comparison of the average of measured fiber stresses in the bridging zone of fatigue cracks to fiber stresses calculated assuming that stress in the bridging zone was uniform.

3. THE EFFECT OF FIBER ARCHITECTURE ON FATIGUE AND FRACTURE OF CERAMIC MATRIX CONTINUOUS FIBER COMPOSITES

The work summarized in this section was presented at a recent ASTM workshop [7]. An appropriate journal will be sought for publication of a more complete version of this work.

Introduction: The objective of this paper is to compare the effects of the failure processes experimentally observed for ceramic matrix composites having several different fiber architectures. The results of experiments are presented with a minimum of analysis due to the diversity of failure modes encountered and the ongoing nature of the research. The reader will note that comparison is made, where appropriate, to the behavior of metals and metal matrix composites because failure modes in those materials have been studied in more detail and are thus more familiar. A secondary objective of this study has been to relate fatigue and fracture properties with the different manufacturing technology used to fabricate each composite.

The composites studied were: (1) a glass-ceramic matrix reinforced with unidirectional Nicalon fibers, (2) a silicon nitride matrix reinforced with SCS-6 fibers, and (3) a silicon nitride matrix reinforced with woven Nicalon fibers. The differing architecture of reinforcing fibers in these composites required that different synthesis routes be used in their manufacture. Composition and fabrication information for each material is summarized in **Table 1**.

Differences in fabrication methods recognize that there were differences in the characteristics of both fiber reinforcement and matrix. The stiffness and strength of the large diameter SCS-6 fibers allowed matrix material to be hot pressed around the fibers, while the close spacing of fibers in the woven Nicalon fabric required that the matrix be of low viscosity so that it could be squeezed into the reinforcement structure. The fabric could not have been infiltrated with glass because of the need to weave the fibers after passing them through the glass frit bath. Similarly, the SCS-6 fibers cannot be woven because of their large diameter.

Thus, a comparison can be made between two materials reinforced with Nicalon fibers (about 20 μm in diameter), but in two different fiber configurations - unidirectional vs. woven material. However, the matrix materials are also different: CAS (a glass-ceramic) vs. fine polycrystalline Si_3N_4 with sintering aids. The other comparison is between small vs. large

diameter unidirectional fiber materials, but having two different matrices.

Table 1
Composition and Fabrication of
Ceramic Matrix Composite Materials

Material No.	Reinforcing Fiber	Matrix	Fabrication Method
1	Nicalon	CAS glass ceramic	Liquid phase sintering of glass powder carried into composite from a slurry.
2	SCS-6	Si_3N_4	Powered matrix was hot pressed around four layers of fibers.
3	Nicalon Fabric	Si_3N_4	Fabric (8 Harness Satin Weave) layers were infiltrated with polymer precursor, which was then pyrolized to Si_3N_4. Eight infiltrations achieved near complete density.

Fatigue and Fracture of Unidirectional Nicalon/CAS Composite

This material was tested for General Electric Aircraft Engine Co. and is included here so that the comparisons discussed above can be made. Detailed results for this materials are in press [8].

This material, a calcium aluminosilicate glass ceramic matrix reinforced by Nicalon fibers, was manufactured by Corning Glass Works. A volume fraction of fibers measured was 0.42, and the average fiber diameter was 16 μm. Two types of fatigue experiments were attempted on this material: (1) Smooth-sided specimens were cyclically loaded at various stress levels until fracture, and (2) notched specimens were cyclically loaded for crack growth rate determination. A stress ratio of R = 0.1 was used for all experiments.

Both single edge notched and center notched specimen geometries were tried for crack growth rate determination, but after an extensive effort to grow cracks perpendicular to the fiber direction in both specimen designs, it was concluded that a dominant crack could not be grown from a notch in this material. Rather, cracks would initiate from the notch, grow in the direction

perpendicular to the loading axis for a short distance, then turn 90° and grow only in the fiber direction. The photographs of **Fig. 1** show this sequence of events. The matrix cracks seen near the notch on the first cycle in Fig. 1 resulted from loading the specimen in bending with a point load at the notch end and supports along the flat side of the specimen. The cracks seen initiated on the tension side of the specimen and must be superficial because no crack opening displacement (COD) was detected during subsequent tensile loading. Also, application of many thousands of cycles did not cause a COD to develop for these cracks. Crack growth behavior similar to that observed here was reported for this material by Luh, et al. [9]. The behavior of this composite has not been seen before in the many notched composite and monolithic materials that have been used for crack growth rate determination, as reported in the literature and in the experience of this investigator. In other words, this behavior is unique.

The stress-life relationship for smooth sided specimens is shown in **Fig. 2**, which also includes data from Butkus and Zawada [10] that was used to establish the approximate fatigue limit. Except for the very small exponent, the relation between stress and cycles looks much like that for a metal.

A detailed examination of the failure sequence was made by loading specimens within the SEM. These observations indicated that failure occurred through the formation of numerous microcracks within the first few loading cycles, but as the number of cycles increased, one of these cracks dominated; i.e., it exhibited a continuously increasing COD that exceeded the opening of other cracks. Examples of this behavior are shown in **Fig. 3**. Although the fiber COD is greater than that of the matrix in Fig. 3(a), the rate of increase in COD is about the same with increasing cycles. The numbers (1), (2), etc., show locations where COD was measured at both maximum and minimum load; very little recovery of COD occurred on unloading. This behavior is a manifestation of "cyclic fiber pull-out," i.e., a ratcheting of the fiber pull out with increasing cycles. The effect of stress level on COD increase, Fig. 3(b), does not seem to be as important as location of the crack, as shown in Fig. 3(c).

A sequence of photographs depicting the behavior of crack density and COD is shown in **Fig. 4**. The specimen failed one cycle after the last photograph was made. A tensile specimen was used to determine the level of stress required to cause matrix cracking; the specimen shown in Fig. 4 was cycled at approximately that stress level. Some cracks were found within the first few cycles, but many others gradually developed as cycling continued, with a near-equilibrium in crack density by 300 cycles. The density then remained

nearly constant until the number of cycles approached that for failure, then the density increased rapidly. Note that the COD of the main or dominant crack increased as the number of cycles increased.

At the higher stress levels, cracks appeared to traverse the entire specimen within one, or at least a few, cycles, while at lower stress, the crack in pattern was more complex. Short segments of crack would appear early in cyclic history, grow in length slowly and stop; meanwhile, the crack density was increasing, and COD of some cracks was increasing. It is likely that the increase in crack density was at least partly responsible in relieving the stress driving the cracks that ceased to grow. It was not possible to obtain useful crack growth data from these experiments.

Fatigue and Fracture of Unidirectional SCS-6/Si_3N_4 Composite

The material tested was fabricated by Textron Specialty Materials by hot pressing silicon nitride powder around the large (150 μm) SCS-6 fibers, also a Textron product. The resulting composite panel had a fiber volume fraction of 0.16, and was so fragile in the transverse direction that careful handling was required. The objective was to obtain crack growth rate data comparable to those obtained for a composite of the same architecture having a matrix of Ti-6Al-4V.

A center notched specimen design was chosen to minimize bending, therefore debonding, that would probably have occurred with either CT or SEN specimens. The specimens were non-conducting; thus, an ultrasonic knife was used to cut the center notches, which were approximately 0.5 mm wide by 8 mm long in a specimen 25 mm in width. Various methods of brazing were attempted for attaching loading tabs, but all these efforts failed. Finally, steel end tabs were attached using epoxy. The three specimens that were fabricated and tested are shown in **Fig. 5**. Both sides of each specimen are shown; specimens were rotated about their long axis.

The loading history of two of these specimens was complex, and despite considerable cracking, remain in one piece. The other specimen was broken in just 200 cycles. The loading histories are shown in **Fig. 6**. Also shown are data derived from Holmes [11] for the same material. From this history, it is possible to obtain an estimate of the stress-life (S-N) relation for this material, as shown in the figure. This may be compared to that found for the Nicalon/CAS composite shown in Fig. 2.

Cracks initiated from the notch, as desired. However, they rarely grew perpendicular to the loading axis, as easily seen for the specimen broken under the largest load. The angles between the loading axis and the crack directions were measured and are listed in **Table 2.**

Table 2
Crack Plane Angles

Specimen	Stress Level (MPa)	No. cycles	Angles (°)	Average Angle (°)
382	117 MPa	200	29,32,33,34	32
385	40	21000	32, 64, 85	60
389	30	6 million	32, 37, 53, 62, 70	50

Newaz and Majumdar [12] have examined the cracking of titanium alloy matrix composites around a hole centered in a tensile specimen. They determined the stresses in the axial (σ_{xx}), longitudinal (σ_{yy}), shear stress (σ_{xy}) and the Hencky-von Mises yield criteria as a function of angle from the direction of loading. The stress showing the greatest correlation with the observed angles was the Hencky-von Mises yield criteria which had a strong maximum at about 70°. Their experimental results showed that cracks initiated at angles of 65-72° to the loading axis. As seen from the above results, the angles predicted by this analysis are greater than those observed for crack initiation from a slit.

As the cracks grew, it was typical for pieces of matrix to fall out, exposing fibers. This can be seen in Fig. 5 and in the closer view of **Fig. 7**. It should be noted in Fig. 7, that the exposed fibers no longer have their outer coating, which, presumably, adhered to the portion of matrix that was lost. When the edge of the specimen was examined, it was evident that multiple cracks had formed through the thickness, so that the cracking pattern observed on each side of the specimen probably was not representative of the crack path in the inner layers in the composite.

Some crack growth rate data were obtained despite the unusual cracking patterns observed. Although these data are very sparse, **Fig. 8**, they indicate a

decrease in crack growth rate with increasing crack length, which is a typical observation made from a SCS-6/Ti-6Al-4V composite of similar architecture [3]. The unbroken specimens were examined for broken fibers, but none was found, although surface damage to fibers, such as shown in Fig. 6, was extensive.

Specimens were loaded inside the SEM and the cracks were examined at various locations. The observation of COD due to loading was location dependent. COD was found for some parts of the crack, but at other locations, loading did not result in a measurable COD. The occurrence of COD on loading is indicative of debonding and slip across the fiber/matrix interface away from the plane of the crack [3], so the absence of COD is an indication that matrix cracking did not always result in slippage between the fiber and matrix. This is opposite of the experience with fatigue crack growth in SCS-6/Ti-6Al-4V composites where an increase in COD always accompanied cracking.

Comparison of these results with Nicalon/CAS indicates that the mechanism of damage tolerance is the same but the cracking behavior is very different; however, a direct comparison is not possible because cracks could not be grown from a notch in the Nicalon/CAS. Fiber bridging of matrix cracks provided the resistance to fracture for both composites. The S-N behavior of Nicalon/CAS was provided by the kinetics of fiber debonding, fracture, and pull-out. Matrix cracking, which was directly connected to fiber failure, varied with stress and cycles. For the SCS-6/Si_3N_4 composite, S-N behavior was provided by crack growth through the matrix, which is at least partially controlled by crack bridging. Matrix cracking appears to be layer selective, thus forming a complex cracking pattern. The narrow range in stress between massive fiber failure and the complete lack of fiber failure for this material led to a slope in the failure line of between - 0.053 and -0.08. The slope of the S-N curve for Nicalon/CAS was approximately the same (-0.065), but for this material, the low slope is due mainly to the sensitivity to stress of the fiber pull-out rate.

The damage tolerence of this composite has been verified by Xu, et al. [13] who found, though 4-point flexure tests, that the failure mode was non-catastrophic between ambient and 1500°C. An increase in fiber volume fraction caused the composite to exhibit an increase in displacement before failure. As temperature was increased, displacment at failure was decreased.

In summary, this composite exhibited non-linear stress-strain and fatigue properties similar in some aspects to metallic specimens. The bridging of

cracks by fibers contributed to this behavior. Some similarity was found for fatigue crack growth between this ceramic matrix composite and metal matrix composites of the same fiber architecture.

Fatigue and Fracture of Nicalon Fabric/Si_3N_4 Composite

The composite material tested was fabricated at Southwest Research Institute using a unique organometallic polymer [14] with a viscosity low enough to be infused into the openings of the woven fiber bundles, or tows. Nicalon fibers coated with carbon and woven into plain and 8 harness satin weaves were purchased from Dow Corning Corp. Individual layers of fabric were coated with polymer; layers were stacked upon one another, bagged, and evacuated during heating to 800°C where polymer pyrolysis occurred. Eight infusion-pyrolysis cycles were required to obtain a near full density material. Composite panels approximately 7 by 13 cm by 3 mm thick were made using this process.

Subsized compact tension specimens (approximately 2 cm square) were cut from the panels and cyclically loaded in compression-tension (R = minimum load/maximum load = -10) until fatigue cracks were initiated. A single crack grew from the notch and was then extended for about 2 mm under constant load until the growth rate approached zero. The procedure used for precracking is the same as had been used successfully for metallic and intermetallic specimens. This behavior indicates that fatigue crack growth in this composite is likely to be similar to that observed for metallic and intermetallic materials.

The first goal of the experimental program was to assess material quality by measurement of fracture toughness. One test was made at ambient temperature and one at 800°C. The cracked specimens were loaded in tension using the SEM loading stage. First the load required to open the crack to the tip was measured, and from this an estimate of $\Delta K_{threshold}$ was made. Next the load was increased until crack growth began. Photographs were made after each increment of load application until rapid crack growth occurred. Crack length and load were then used to compute the fracture toughness using formulae found in ASTM standards. **Fig. 9** shows how these data may be used to estimate the tension-tension fatigue crack growth characteristics of this composite. Of course, this estimate must be further examined by actual experimental measurements of fatigue crack growth, but the similarity with the behavior of metallic materials is very interesting.

The DISMAP system was used to measure displacements in material ahead of the crack tip and in unbroken fibers that bridged the crack before tearing began and just before rapid fracture began. From measured displacements, COD along the crack wake and strains surrounding the crack tip were determined. Shown in **Fig. 10** are the displacements overlaid on the microstructure of the composite, COD, and the maximum shear strain in the region ahead of the crack tip. The material response characteristics to note from this analysis are: (1) the symmetry of displacements relative to the crack line, (2) the sharpness of the crack tip as determined from the COD measurements, and (3) the lack of strain concentration caused by the crack tip. In fact, strain is somewhat larger approximately 25 μm ahead of the crack tip than it is at the tip. This material deformation is quite different from that found for crack tips in metals where displacements are almost always found to be asymmetric about the crack plane, and the maximum strain occurs at the crack tip.

Conditions at the crack tip are somewhat different for a load only a few Newtons below that required for rapid fracture, as shown in **Fig. 11**. The material has responded with a less symmetrical displacement field, the crack tip is now blunted, as shown by COD measurements, and the strain is larger, but still not concentrated at the tip. Fibers ahead of the crack tip have not debonded, and a few fibers in the crack wake have not yet broken.

The low magnification view of the broken specimen shown in **Fig. 12** indicates significant fiber pull-out in the region of cyclic crack growth, but little fiber pull-out in the region of rapid crack growth. The fiber pull-out distance was about 200 μm near the notch (the region of higher crack growth rate) and increased to about 350 μm as the crack growth rate decreased farther away from the notch, as is characteristic for cracks grown using compression loading. In the zone of fast fracture, only a very small amount of fiber pull-out was found.

Fracture toughness for this lot of material was approximately 15 MPa$\sqrt{m}$ at ambient temperature and 14 MPa$\sqrt{m}$ at 800°C. Tensile tests of this material are still being conducted, but a preliminary test at 800°C indicated that the yield stress was about 115 MPa, with an ultimate stress of about 130 MPa and a "strain" to failure of about 0.017. This strain was only apparent; the elongation consisted mainly of the COD of cracks within the gage section of the specimen.

The unit cell size [15], or repeat distance within the fabric, for this composite is approximately 10 mm square. The tensile test was conducted on a

specimen much smaller than the unit cell size, and may, therefore, not be representative of the material. Conversely, the CT specimens used for fracture were twice as large as the unit cell size. Unit cell size is an important dimension for textile reinforced composites because it forms the basis for models of elastic modulus and Poisson's ratio [16]. However, the results of fracture experiments show that unit cell size is much too large to be used as a basis for models of fatigue and fracture toughness because the amount of material responding to the crack presence is much smaller than the unit cell size, even if the length of fiber pull-out is included.

Comparative Analysis and Discussion of Fiber Architecture Effects

The reason for making ceramic matrix composites is to achieve non-catastrophic, or "graceful" failure, instead of the catastrophic fracture that usually accompanies monolithic ceramics. All of the composites studied have achieved this goal, as directly observed from (1) the tensile stress-strain behavior, (2) the S-N behavior of Nicalon/CAS and SCS-6/Si_3N_4, and (3) the fact that both the SCS-6/Si_3N_4 and the Nicalon Fabric/Si_3N_4 composites exhibited crack growth rates similar to those observed for metallic materials. For Nicalon/CAS and SCS-6/Si_3N_4, crack bridging by fibers was a principal cause of the observed behavior, but the results to date for Nicalon Fabric/Si_3N_4 indicate that crack bridging may be the reason for the stress-strain response, but mechanisms other than crack bridging are likely to be responsible for the fatigue characteristics.

The mode of cracking from a slit stress concentration probably provides the most striking difference in the behavior of these composites. In spite of the similarity between fiber diameter and matrix material, cracking of the Nicalon Fabric/Si_3N_4 and Nicalon/CAS composites was completely different. Despite the differences between the Nicalon Fabric/Si_3N_4 and SCS-6/Si_3N_4, cracking was similar. It appears that a model that is capable of incorporating the disparate behavior of these composites will be complex and must incorporate micromechanics as well as continuum mechanics.

4. FUTURE WORK

The work on Nicalon Fabric/ceramic matrix composites will be continued. Experiments will be performed on composites made at Kaiser Ceramic Composites and Southwest Research Institute. Experiments will be designed to determine tensile stress-strain, fatigue crack initiation, fatigue crack growth, and fracture toughness characteristics at ambient and 800°C for these materials, but all these properties will not be measured for each material. It will be necessary to use different specimen designs for each experiment. Stress-strain, S-N, and fatigue crack initiation will use specimens with tapered ends for load transfer to the grips; fracture toughness will be measured using straight notched, 3-point bend bars and compact tension (CT) specimens, and fatigue crack growth will use also use CT specimens. All specimen designs are compatible with our SEM loading stages and laboratory loading frames.

As it now appears, the major challenge for this research will be to derive a method for accounting for the unique behavior of the Nicalon Fabric composites that exhibit a pseudo-plastic behavior; i.e., these materials show behavior that looks like plasticity, but the system consists of a brittle fiber incorporated in a brittle matrix. Unreinforced fabrics exhibit "ductility" because the fibers can move relative to one another and exhibit shear; thus, they can be draped easily to conform to a part shape in a manufacturing process. The incorporation of matrix makes the composite stiff by preventing fiber shear, but the material still exhibits relatively large shear strains in the vicinity of a loaded crack tip with an absence of crack bridging. Thus, it is the shear that must account for the high toughness observed. The objectives of future research will be to describe the observed behavior, and to try to use this information to produce higher strength, more damage tolerant materials.

5. REPORT REFERENCES

1. D.L. Davidson "Fiber-matrix micromechanics and microstructural observations under tensile and cyclic loading" in **Prediction Methodology for Titanium Matrix Composites**, ASTM-STP (in review)
2. D.L. Davidson "The micromechanics of fatigue crack growth at 25°C in Ti-6Al-4V reinforced with SCS-6 fibers" **Met. Trans. A.**, v. 23A, 1992, pp. 865-879.
3. D.L. Davidson "The effect of fiber architecture on fatigue and fracture of ceramic matrix continuous fiber composites" (in preparation)

4. R. John, J.R. Jira, J.M. Larsen and N.E. Ashbaugh "Fatigue crack growth in unidirectional SCS-6/Ti-24Al-11Nb composite containing a circular hole (Part II), **Metall. Trans. A**, 1994 (in press).
5. D.L. Davidson "Fatigue crack growth through ARALL-4 at ambient temperature" **Fatigue Fract. of Engng. Mater. Struct.**, v. 14, 1991, pp. 939-951.
6. D.L. Davidson "Fatigue crack growth through composites with continuous fiber reinforcement" **ICCM/9 Conf. Proceedings, Vol. I**, A. Miravete, ed., U. Zaragoza & Woodhead Publ. Ltd., 1993, pp. 571-577.
7. "Fatigue of Ceramic Matrix Composites" organized by Noel Ashbaugh and Mike Mitchell and held at DFW airport on Nov. 15, 1993.
8. C.Q. Rousseau, D.L. Davidson, and J.B. Campbell "The micromechanics of ambient temperature cyclic fatigue loading in a composite of CAS glass ceramic reinforced with Nicalon fibers" **J. Composites Tech. & Research (ASTM)**, 1994 (in press).
9. E.Y. Luh, R.H. Dauskardt, and R.O. Ritchie "Cyclic fatigue crack growth behavior of short cracks in SiC reinforced LAS glass ceramic composite" **J. Mat. Sci. Letters**, v. 9, 1990, pp. 719-725.
10. L.M. Butkus, L.M. Zawada and G.A. Hartman "Room temperature tensile and fatigue properties of silicon carbide fiber reinforced aluminosilicate glass" **J. Am. Ceram. Soc.**, v. 74, 1991, pp. 2851-2858.
11. J.W. Holmes "Fatigue of fiber reinforced ceramic composites" in **Ceramics and Ceramic Matrix Composites**, S.R. Lavine, ed., ASME, 1992, pp. 193-238.
12. G.M. Newaz and B.S. Majumdar "Crack initiation around holes in a unidirectional MMC under fatigue loading" **Eng. Fract. Mech.**, v. 42, 1992, pp. 699-711.
13. H.H.K. Xu, L.M. Braun, C.P. Ostertag, R.F. Krause, and I.K. Lloyd "Failure modes of SiC-fiber/Si_3N_4-matrix composites at elevated temperatures" **J. Am. Ceram. Soc.** (in press) 1994.
14. S.T. Schwab, R.C. Graef, D.L. Davidson, and Y.Pan "Applications of polysilazanes as precursors to silicon nitride" **Polymer Prepreints**, v. 32, 1991, pp. 556-558.
15. T-W. Chou and T. Ishikawa "Analysis and modeling of two-dimensional fabric composites" in **Textile Structural Composites** T-W. Chou and F.K. Ko, eds, Elsevier, New York, 1989, pp. 209-264.
16. N.K. Naik and V.K. Ganesh "Prediction of on-axes elastic properties of plain weave fabric composites" **Comp. Sci. and Tech.**, v. 45, 1992, pp. 135-152.

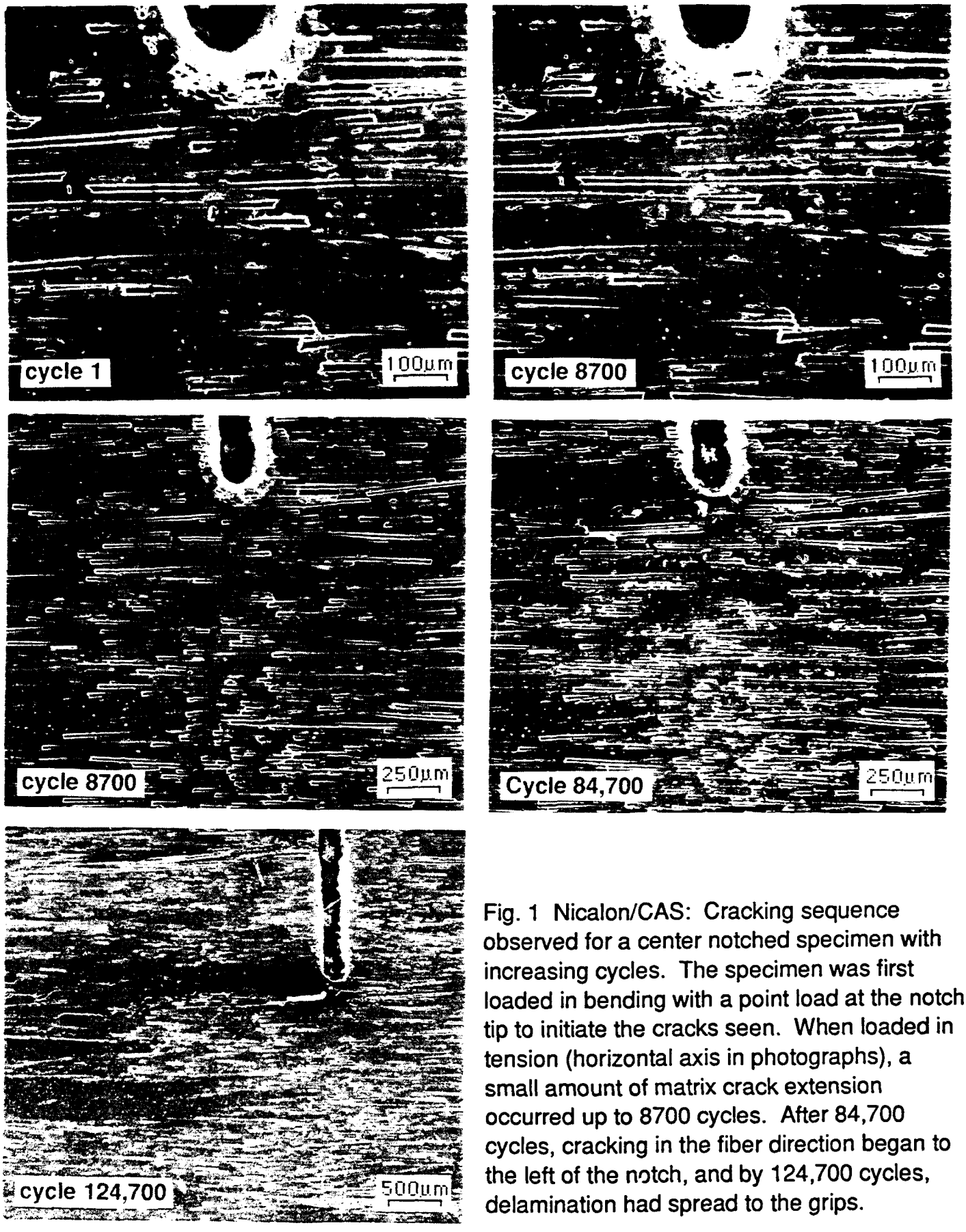

Fig. 1 Nicalon/CAS: Cracking sequence observed for a center notched specimen with increasing cycles. The specimen was first loaded in bending with a point load at the notch tip to initiate the cracks seen. When loaded in tension (horizontal axis in photographs), a small amount of matrix crack extension occurred up to 8700 cycles. After 84,700 cycles, cracking in the fiber direction began to the left of the notch, and by 124,700 cycles, delamination had spread to the grips.

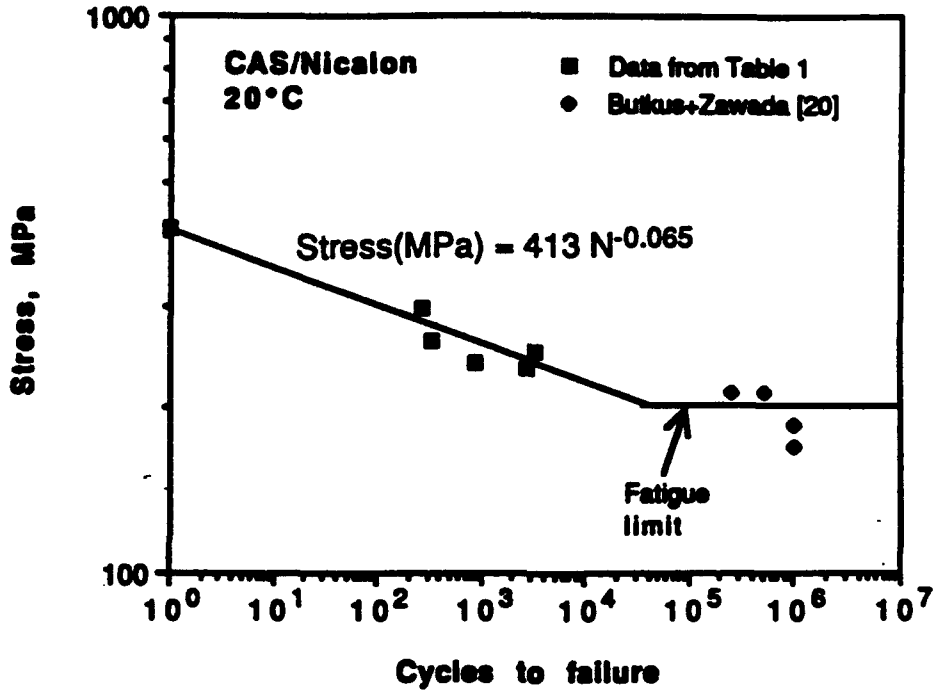

Fig. 2 Nicalon/CAS: The effect of stress on the number of cycles required to fracture smooth specimens at R = 0.1.

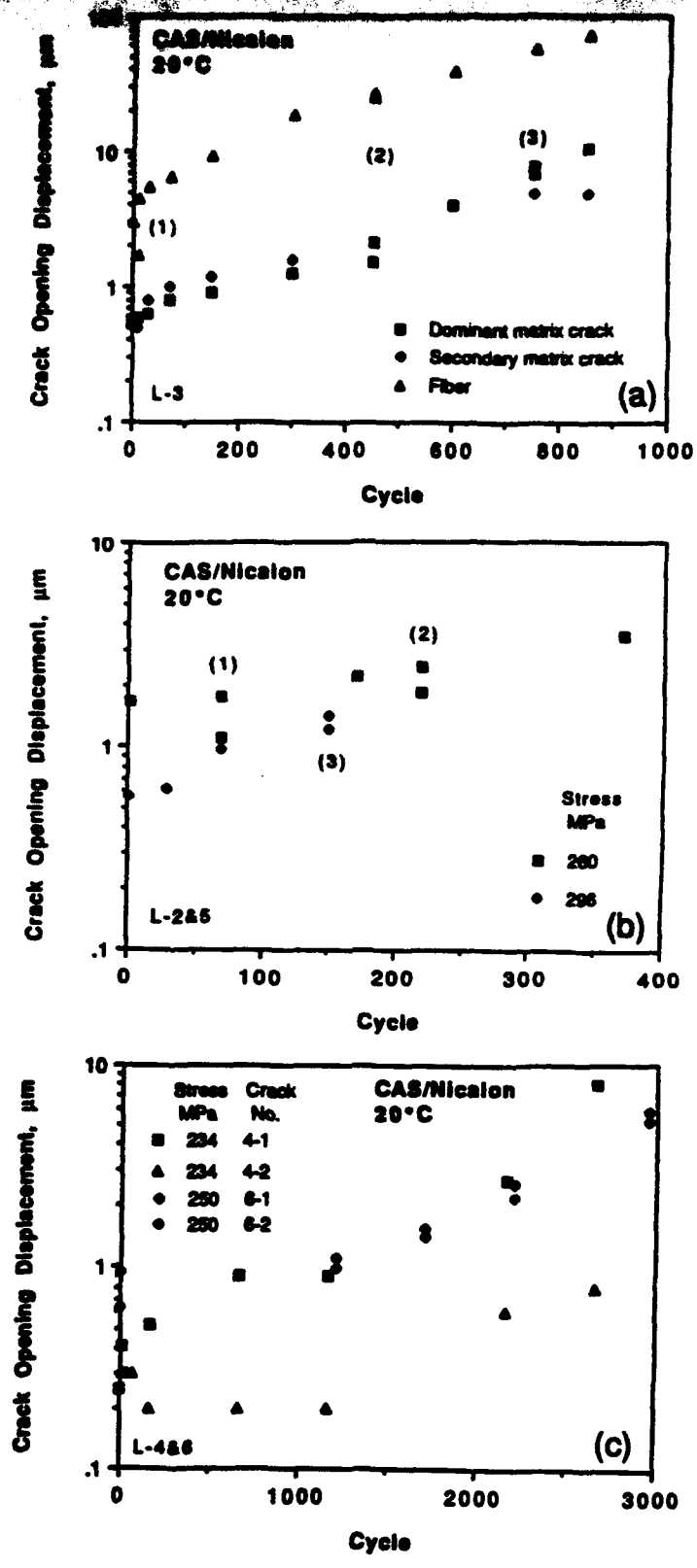

Fig. 3 Nicalon/CAS: The change in COD with loading cycles. (a) COD in matrix and fibers for a stress range of 276 MPa. Note that COD of the fiber crack is considerably larger than for the matrix cracks. (b) COD for matrix cracks at stress ranges of 260 and 296 MPa. Numbers in () indicate the change in COD caused by unloading to minimum stress. (c) COD for a stress range of 234 and 250 MPa. The two cracks at 250 MPa have about the same COD while the two cracks at 234 MPa have very different COD.

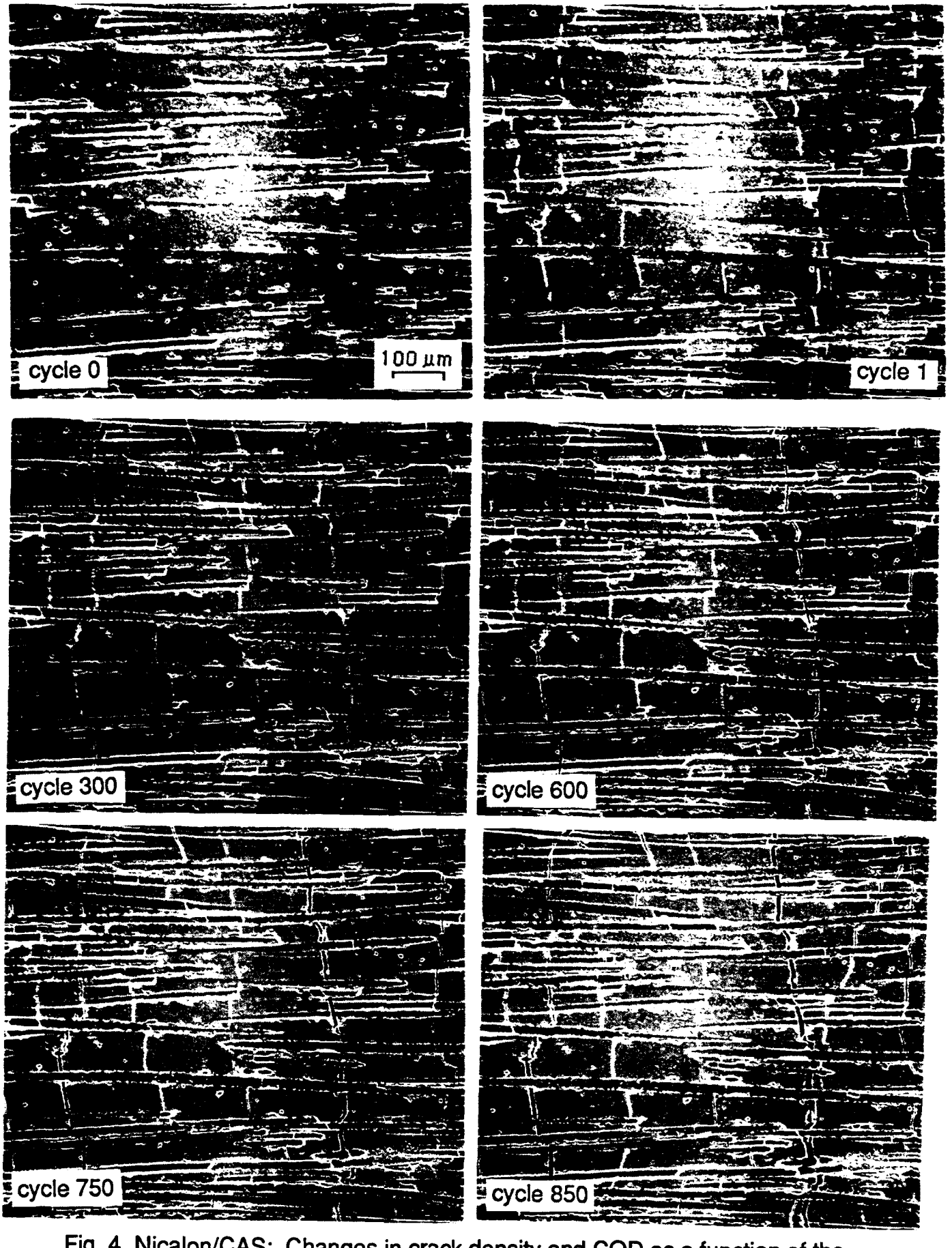

Fig. 4 Nicalon/CAS: Changes in crack density and COD as a function of the number of loading cycles. Stress range = 238 MPa.

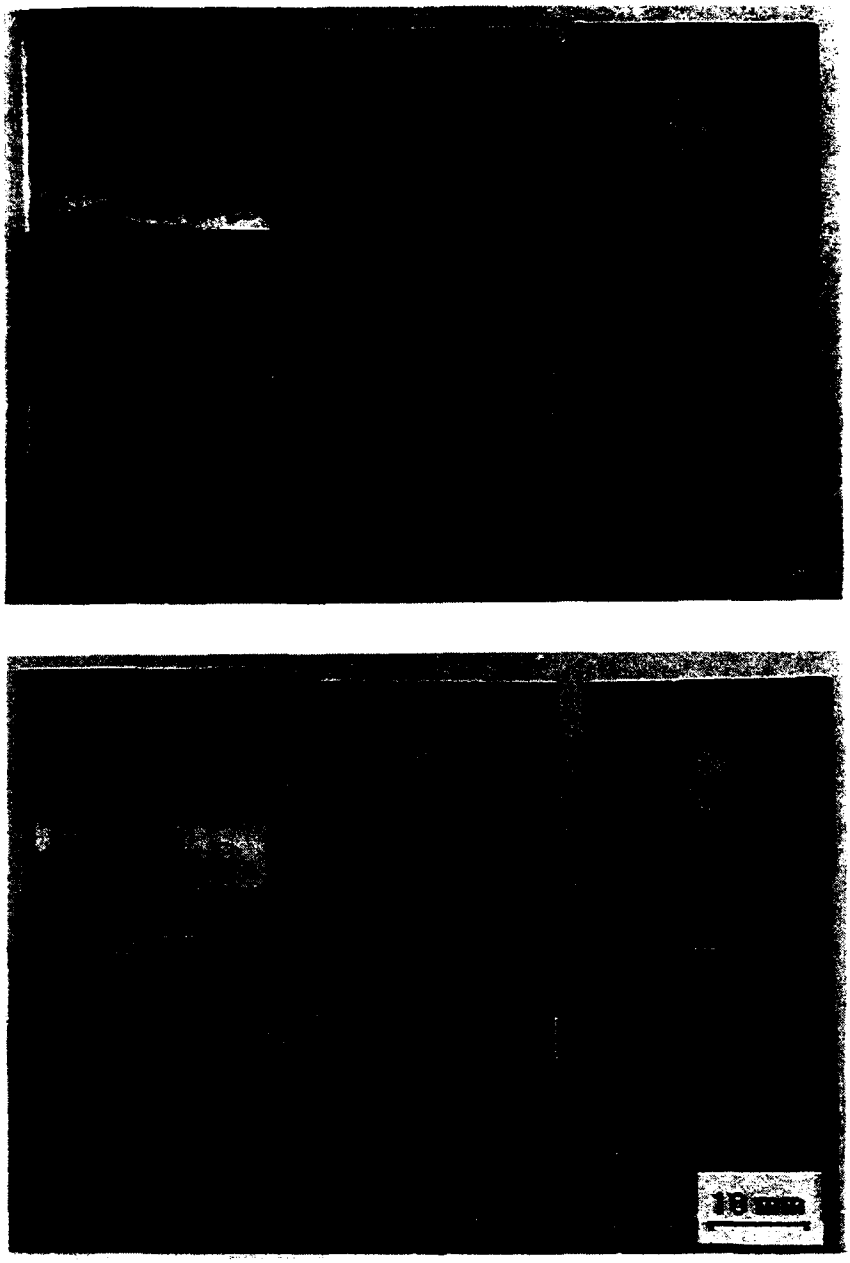

Silicon nitride/SCS-6 composites formed from hot pressed powders.

Spec.	382	117 MPa	200 cycles	fractured
	385	40-80	21,000	unbroken
	389	30	6 million	unbroken

Fig. 5 SCS-6/silicon nitride: Specimens tested (#382) at 117 MPa for 200 cycles - broken, (#385) 40-80 MPa for 21000 cycles, and (#389) at 30 MPa for 6 million cycles (last 2 unbroken).

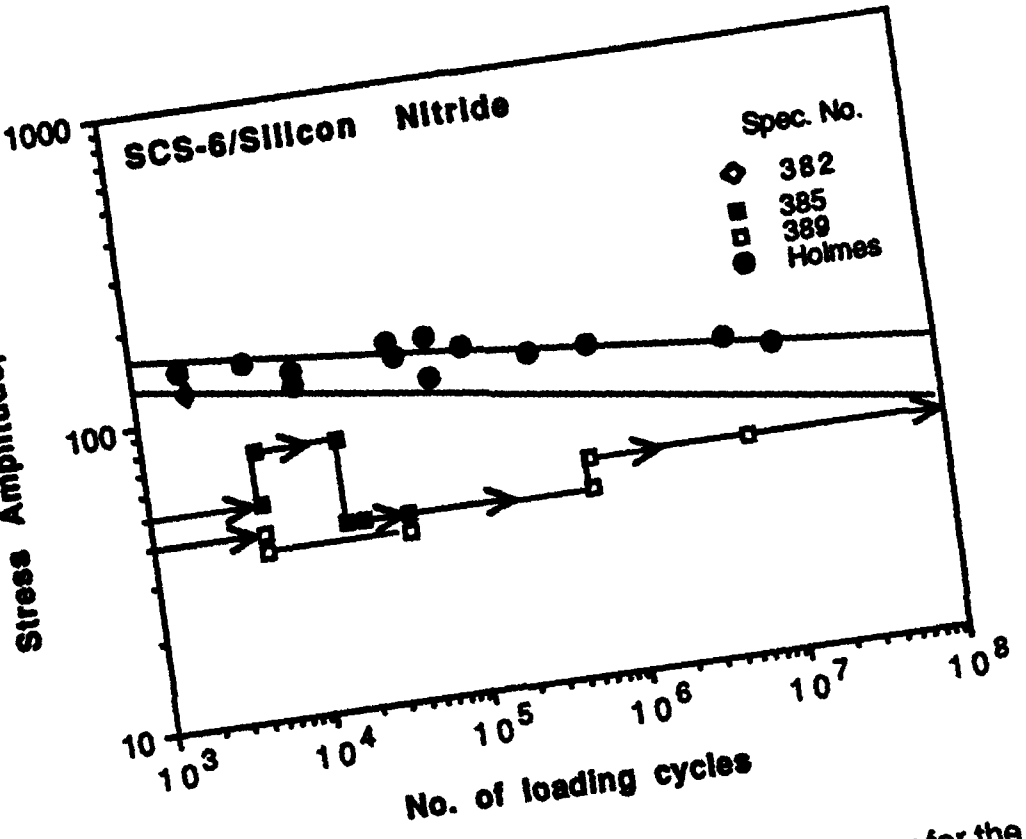

Fig. 6 SCS-6/silicon nitride: Stress-lifetime and stress history for the specimens tested. Results are compared with those given in Holmes [11] which were derived from unnotched specimens. Exponents in the equation $\sigma = \sigma_o N^m$ are $m = 0.053$ for the upper curve and $m = 0.08$ for the lower curve.

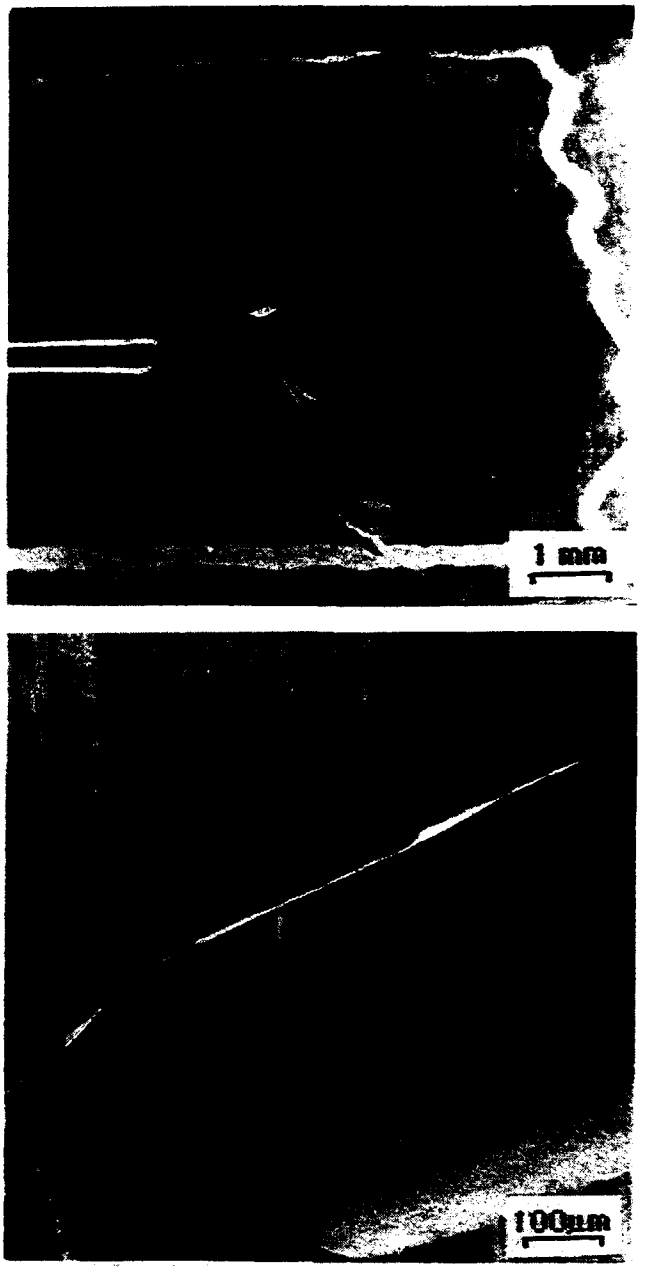

Spec. 385: 21,000 cycles at 40-80 MPa.

Fig. 7 SCS-6/silicon nitride: Details of the cracking that occurred in the specimen cycled at 40 to 80 MPa for 21000 cycles showing matrix spallation.

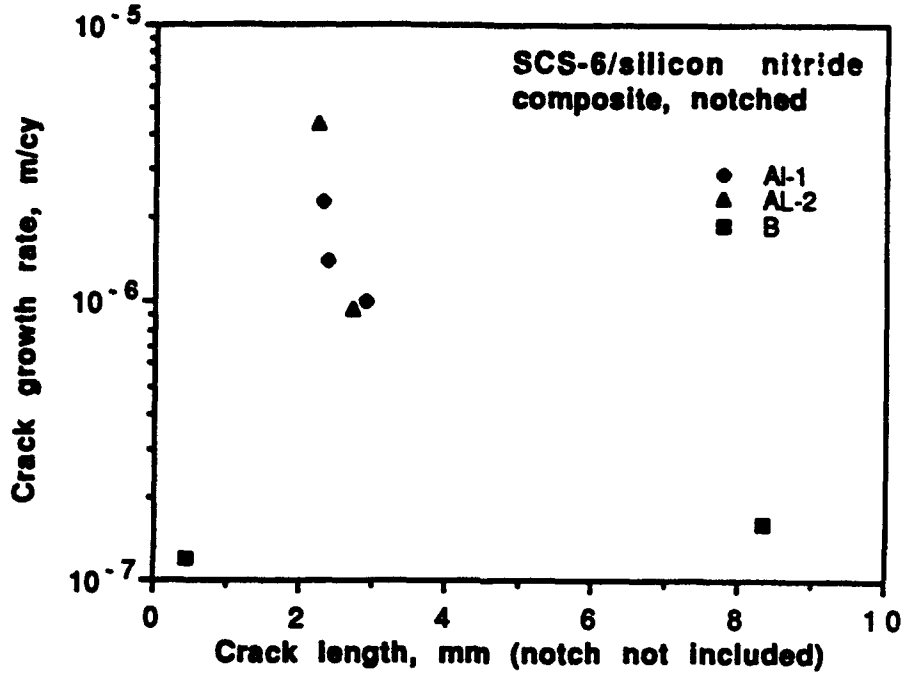

Fig. 8 SCS-6/silicon nitride: Crack growth rate as a function of crack length showing that the rate decreased as the crack length increased.

Estimate of Fatigue Crack Growth Characteristics for the Nicalon Fabric/Si_3N_4 Composite at 25°C

1. At minimum load (36 N) the fatigue crack was tightly closed.
2. Crack opened to the tip upon loading to 170 N
3. Maximum load for fatigue precracking was 300N. This load corresponded to K_{max} = 4.4 MPa$\sqrt{m}$.
4. At fracture, the load was 536 N, after a crack growth of 0.5 mm. This condition corresponded to K_c = 15.6 MPa$\sqrt{m}$. The crack was assumed to be growing at ≈ 10^{-6} m/cy when fast fracture began.
5. At the load just required for crack opening, $U = (1-P_o/P_{max})/(1-R)$ = 0.481, a value of threshold can be estimated by setting $U = 1 - (K_{th}/K_{max})$. This gives a value of K_{th} ≈ 2.28 MPa$\sqrt{m}$. At threshold, the crack had approximately stopped growing; therefore, da/dN ≈ 10^{-12} m/cy.
6. Using the above values of K and da/dN, the crack growth rate curve ($da/dN = B K_{max}^{s}$) may be estimated, as shown below, giving B = 2.7x10^{-15} m/cy and s = 7.2.

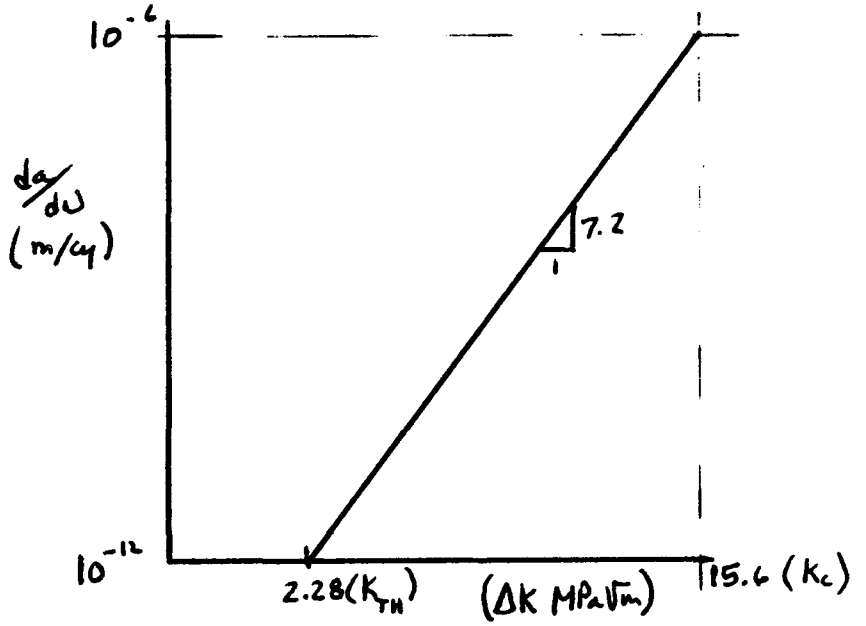

Fig. 9 An estimate of the expected crack growth rate curve for the textile reinforced composite

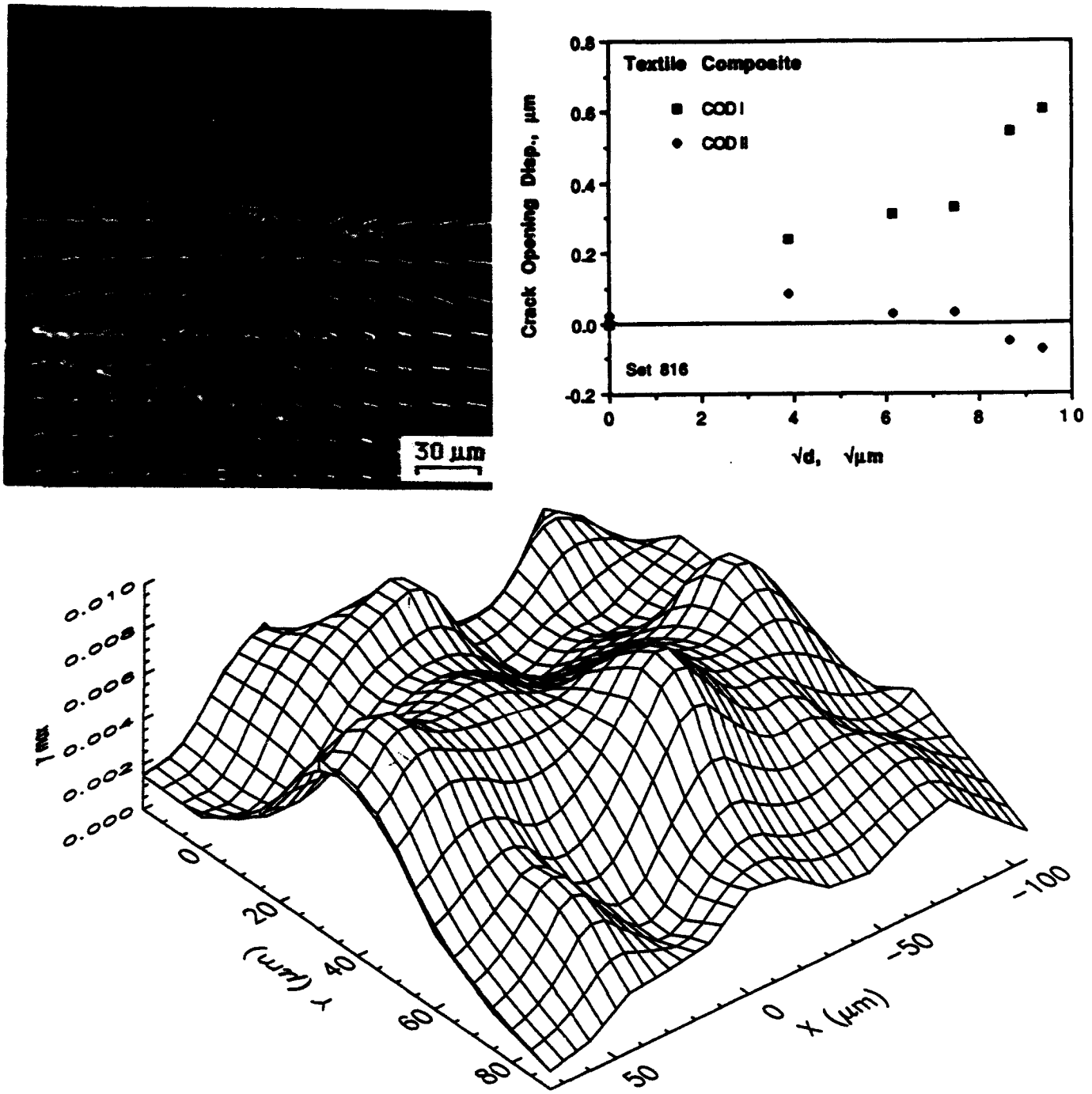

Fig. 10 Nicalon fabric/silicon nitride: Compact tension specimen loaded (along the horizontal axis) to K = 5.9 MPa√m at 25°C. Fibers seen in the photograph were still bonded to the matrix. Displacements (shown on the photograph) were measured each 15 µm, and the displacement magnitudes are 20 times actual value. The Mode I COD indicates that the crack tip has blunted slightly, and the strain distribution indicates that the strain has been disbursed ahead of the crack tip, thus, minimizing the strain concentration at the crack tip.

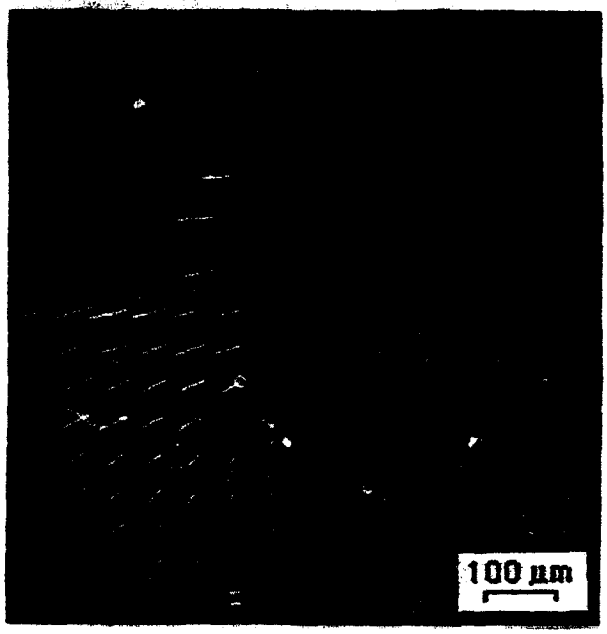

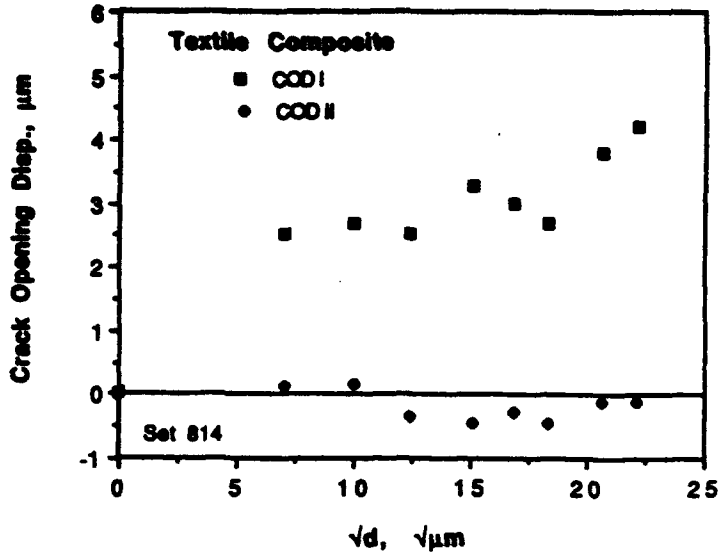

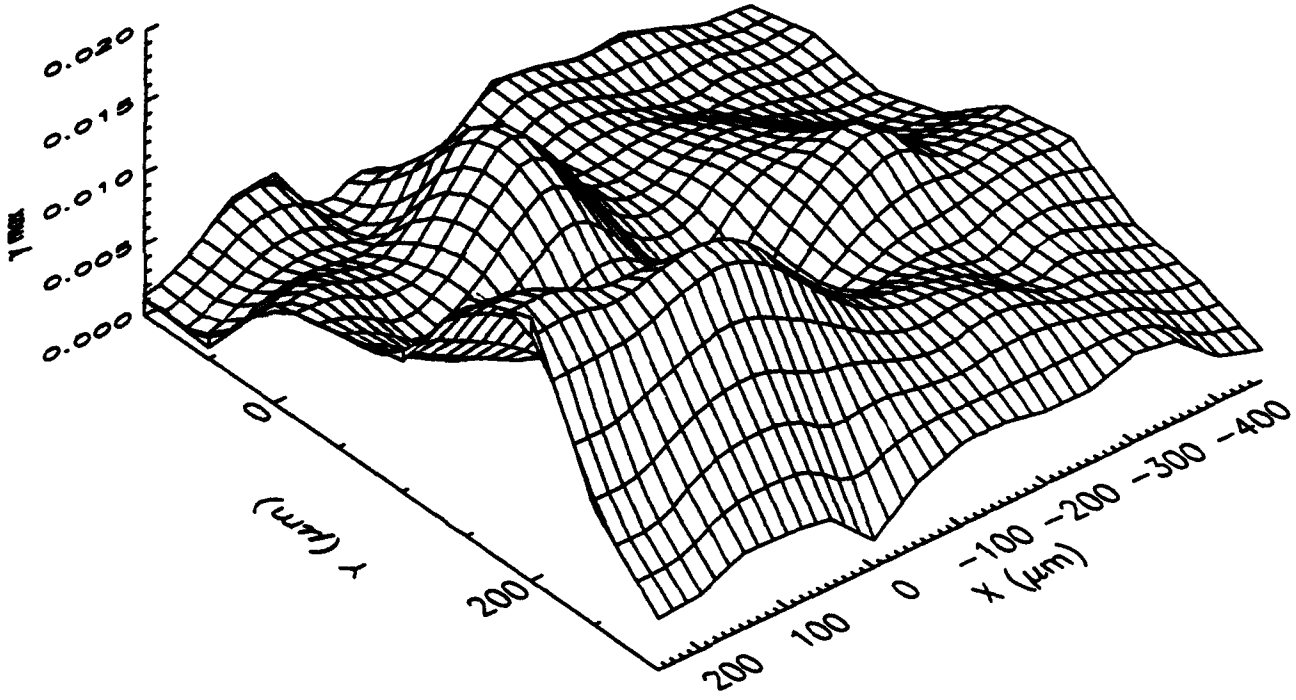

Fig. 11 Nicalon fabric/silicon nitride: Compact tension specimen loaded (along the horizontal axis) to K = 13.8 MPa√m at 25°C. Fibers seen in the photograph were still bonded to the matrix. Displacements (shown on the photograph) were measured each 50 µm, and the displacement magnitudes are 15 times actual value. The Mode I COD indicates that the crack tip is very blunt, and the strain distribution indicates that the strain has been disbursed ahead of the crack tip, thus, minimizing the strain concentration at the crack tip. Some fibers in the crack wake were not broken.

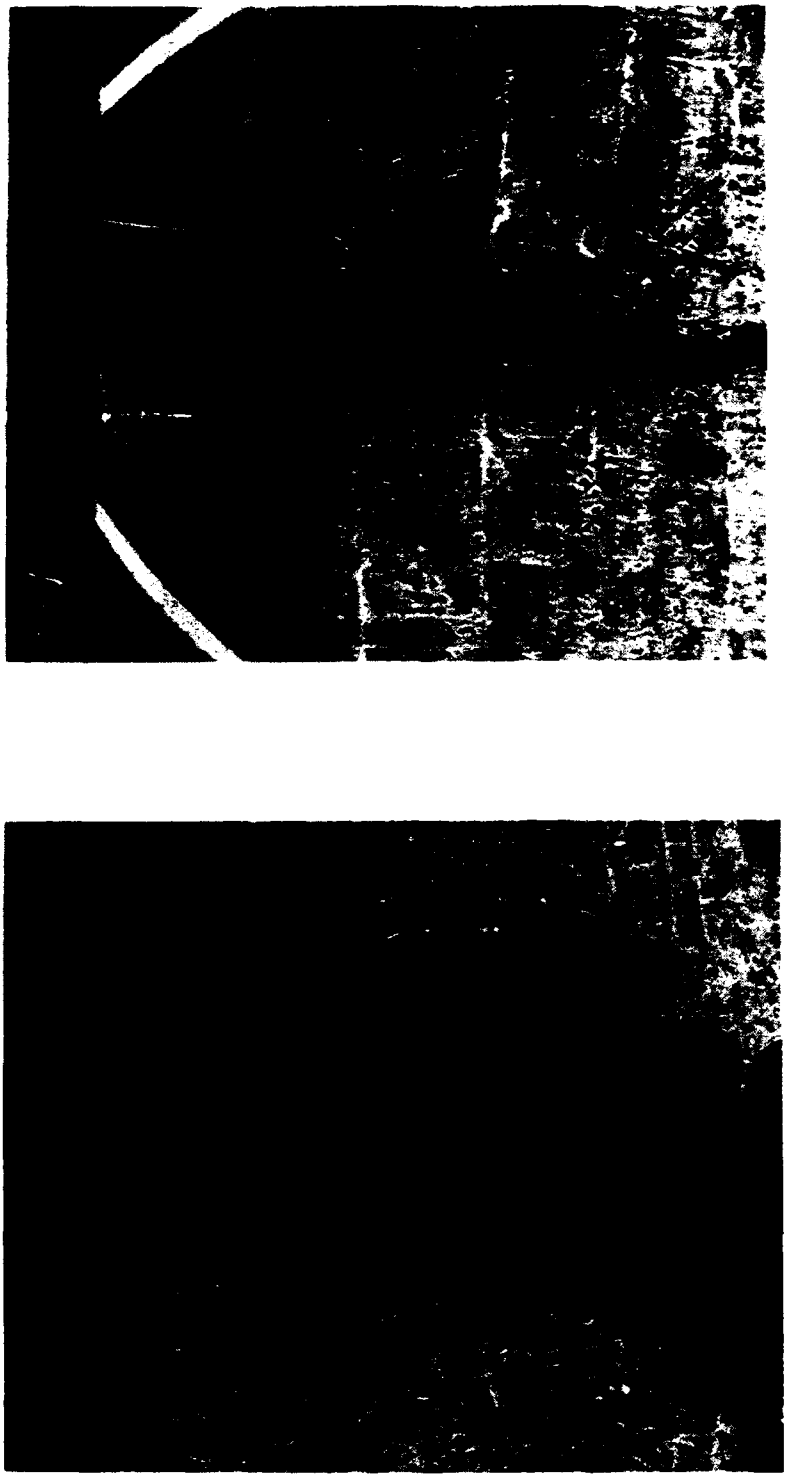

Fig. 12 Nicalon fabric/silicon nitride: A side view of the broken specimen showing fiber pull-out in the fatigue cracked region, but very little fiber pull-out in the fast fracture region.